Synaptic patterning of left-right alternation in a computational model of the rodent hindlimb central pattern generator

William Erik Sherwood · Ronald Harris-Warrick · John Guckenheimer

Abstract Establishing, maintaining, and modifying the phase relationships between extensor and flexor muscle groups is essential for central pattern generators in the spinal cord to coordinate the hindlimbs well enough to produce the basic walking rhythm. This paper investigates a simplified computational model for the spinal hindlimb central pattern generator (CPG) that is abstracted from experimental data from the rodent spinal cord. This model produces locomotor-like activity with appropriate phase relationships in which right and left muscle groups alternate while extensor and flexor muscle groups alternate. Convergence to this locomotor pattern is slow, however, and the range of parameter values for which the model produces appropriate output is relatively narrow. We examine these aspects of the model's coordination of left-right activity through investigation of successively more complicated subnetworks, focusing on the role of the synaptic architecture in shaping motoneuron phasing. We find unexpected sensitivity in the phase response properties of individual neurons in response to stimulation and a need for high levels of both inhibition and excitation to achieve the walking rhythm. In the absence of cross-cord excitation, equal levels of ipsilateral and contralateral inhibition result in a strong preference for hopping over walking. Inhibition alone can produce the walking rhythm, but contralateral inhibition must be much stronger than ipsilateral inhibition. Cross-cord excitatory connections significantly enhance convergence to the walking rhythm, which is achieved most rapidly with strong crossed excitation and greater contralateral than ipsilateral inhibition. We discuss the implications of these results for CPG architectures based on unit burst generators.

Keywords Central pattern generator · Computational model · Locomotion · Rodent spinal cord · Hindlimb · Bursting

W. E. Sherwood (✉)
Center for BioDynamics, Boston University,
111 Cummington Street, Boston, MA 02215, USA
e-mail: wesher@bu.edu

R. Harris-Warrick
Department of Neurobiology and Behavior,
Cornell University, Seeley Mudd Hall, Ithaca,
NY 14853, USA
e-mail: rmh4@cornell.edu

J. Guckenheimer
Mathematics Department, Cornell University,
565 Malott Hall, Ithaca, NY 14853, USA
e-mail: jmg16@cornell.edu

1 Introduction

The neuromuscular system of a walking mammal repeatedly executes a complex sequence of correctly phased contractions and relaxations of more than a dozen muscles in each hind leg, comprising groups of flexors and extensors pulling and pushing at the hips, knees, ankles, feet, and digits (Kiehn and Kjaerulff 1996). The rodent spinal hindlimb locomotor central pattern generator (RSHL CPG), which is primarily active in the lower thoracic and lumbar spinal segments, coordinates the correct phasing of the various leg muscles' activity (flexion-extension) for effective

locomotion. Roughly speaking, during normal locomotion, the flexor muscles of one side of the animal are active out of phase with the flexor muscles of the other side, and there is similar cross-cord alternation of extensor muscle activity. At the same time, the flexor muscles of one side of the animal are active out of phase with the ipsilateral extensor muscles. We call this simultaneous ipsilateral flexor-extensor antisynchrony and contralateral flexor-flexor/extensor-extensor antisynchrony the *fundamental locomotor rhythm* of the RSHL CPG.[1] This behavior is manifest *in vivo* and in experiments *in vitro* in which the spinal cord is removed intact from the rodent and the CPG is activated with neuromodulators. Walking-like phasing of motoneuron activity, monitored from their action potentials in the ventral roots, is known as *fictive locomotion* in these spinal cord experiments (Butt et al. 2002; Kiehn and Butt 2003). Motoneuron activity measured in the ventral roots from the second lumbar spinal segment (the L2 ventral roots) monitors primarily activity of flexor motoneurons, while activity measured in the ventral roots from the fifth lumbar spinal segment (the L5 ventral roots) monitors primarily activity of extensor motoneurons. In isolated spinal cord experiments on rodents, flexor and extensor activation is roughly balanced, with each motoneuron group exhibiting a duty cycle of approximately fifty percent (Butt et al. 2002). Note that sensory feedback is not present in the fictive locomotion studies and that these experiments are usually done with spinal cords of newborn animals that have not begun to walk, so the resetting properties of the fundamental locomotor rhythm in these experiments may differ from the *in vivo* behavior of older animals.

Complementary to these experiments are abstract models of animal gait consisting of coupled oscillators (Golubitsky et al. 1998, 1999). Among the most analytically tractable are "phase oscillator" models that reduce each oscillator to a limit cycle and assume that the coupling between oscillators depends only upon their phase differences. The mathematical theory of coupled cell networks investigates which patterns of synchrony and other phase relationships between cells can arise robustly, purely as a consequence of the network architecture (Stewart et al. 2003; Golubitsky and Stewart 2006), without assuming that the cells' intrinsic dynamics can be described solely in terms of phase. In the context of locomotion, coupled cell network

theory has been used to demonstrate minimal network structures for CPGs that are able to produce all primary and secondary bipedal and quadrupedal gaits (Pinto and Golubitsky 2006; Buono and Golubitsky 2001; Buono 2001). The presence of symmetries in the coupling architecture is essential to the theory, but its results concerning the existence or absence of certain kinds of phase relationships are largely independent of the details of the dynamics intrinsic to each component oscillator in isolation. Though quite powerful for proving an abstract CPG model's capacity to produce particular gaits stably, the theory provides less guidance regarding other questions relevant to modeling locomotor activity, given a concrete choice of oscillator, e.g. for how broad a range of parameters do particular phase relationships persist? How strong (or weak) must synaptic coupling be in order to produce a desired gait? If multiple stable phase relationships are possible for a given set of parameters, how large is each gait's basin of attraction? What kinds of transitions between gaits occur as synaptic coupling strengths change?

This paper presents a modeling study designed to bridge the gap between fictive locomotion experiments and abstract models by investigation of a more experimentally-based model for the RSHL CPG. Our model incorporates biophysically realistic model oscillatory neurons synaptically coupled with an architecture compatible with experimental data and exhibiting a number of symmetries. According to theory, the symmetries present in the coupling network imply that the CPG model should be able to reproduce basic locomotor gaits—but which ones actually appear, how robustly, and for what synaptic strengths?

One important aspect of real CPG activity about which mathematical theory is relatively silent, and which in part motivates this study, is transient behavior. Biological locomotor CPGs have the ability to respond quickly to fast changes in stimulation without extended transients, i.e. they can restore their stable rhythm rapidly following perturbation. An animal must be able to compensate for sudden changes in posture or terrain within a few periods of the locomotor cycle (Hultborn 1998). Such perturbations occur continually during free movement, an environmental constraint that distinguishes the chief functional considerations for locomotor CPGs from those of CPGs governing other rhythmic behaviors, such as digestion, circulation, or, to a lesser extent, respiration. Rapid resumption of the fundamental locomotor rhythm after perturbation (stability) is essential for successful walking movement, as is near-instantaneous adaptation of the rhythm and phasing of neuromuscular output in response to higher order commands and sensory input. The

---

[1] Equivalently described as simultaneous ipsilateral flexor-extensor antisynchrony and contralateral flexor-extensor synchrony.

models we investigate do not have this property, suggesting the need for further study of the resetting properties of fictive locomotion in both experiments and models.

1.1 Rhythmic patterns

Dynamical systems principles identify gaits with symmetry properties of networks of coupled oscillators. Patterned activity in the isolated rodent spinal cord (in preparations where the whole cord is removed from the animal and pharmacologically stimulated) takes four basic forms: total synchrony, rhythmic left-right alternation (ipsilateral synchrony), hopping, and fictive locomotion (Nishimaru and Kudo 2000; Kullander 2005; Dottori et al. 1998). In synchronous activity, motoneurons in the L2 (predominantly flexor-related) and L5 (predominantly extensor-related) segments show regular, periodic bursts of activity, such that motoneurons in L2 fire in phase with motoneurons in L5, and motoneurons on one side of the cord fire in phase with motoneurons from the other side. Rhythmic left-right alternation is marked by ipsilateral intersegmental synchrony between L2 and L5, and intrasegmental alternation of activity between motoneurons on either side of the midline. Hopping is characterized by intrasegmental cross-cord (left-right) synchrony (for example, left and right flexor motoneurons fire synchronously), but alternation of periodic bursts in the ipsilateral L2 and L5 segments. During fictive locomotion, there is both ipsilateral intersegmental and contralateral intrasegmental alternation, meaning that L2 motoneurons on one side of the cord are active out of phase with ipsilateral L5 motoneurons and contralateral L2 motoneurons, but are active in phase with contralateral L5 motoneurons. Fictive locomotion corresponds to a normal walking pattern. Spontaneous spinal activity in intact rodents progresses from synchronous to rhythmic left-right alternation to fictive locomotion as the animals proceed normally through the stages of pre- and post-natal development (Kullander 2005).

A large number of studies have established that a variety of neurotransmitters and other chemical agents, alone or in combination, can elicit locomotor-like patterns in the isolated rodent spinal cord: Serotonin (5-HT), NMDA, NMA, extracellular K^+, dopamine (DA), acetylcholine (ACh), noradrenaline (NA) (Sqalli-Houssaini et al. 1993; Cowley and Schmidt 1997; Bracci et al. 1998; Kiehn and Kjaerulff 1996; Hinckley et al. 2005; Zhong et al. 2006b; Wilson et al. 2005; Hochman et al. 1994; Kiehn et al. 1999; Beato and Nistri 1999). Additional experiments have demonstrated that individual interneurons of the L2 and L5

segments prefer to fire at relatively fixed phases in the locomotor cycle (Tresch and Kiehn 1999; Tresch and Kiehn 2000; Raastad and Kiehn 2000; Beierholm et al. 2001; Zhong et al. 2006a, b). In neonatal animals, gap junctions synchronize local motoneuron pools, while chemical synapses synchronize or antagonize motoneurons in spatially distinct pools (Tresch and Kiehn 2002).

1.2 Neuron types

In our model of the RSHL CPG, we simplify the neuronal organization of the spinal locomotor network to three functional classes: *Motoneurons* (MNs), *commissural interneurons* (CINs), and groups of interneurons that participate in locomotor rhythm generation, collectively called *rhythmogenic interneurons* (RGNs). Motoneurons innervate the muscles of the hindlimbs directly, and their axons form the ventral roots from which recordings of fictive locomotor activity are made. Commissural interneurons have axonal processes which cross the midline of the spinal cord; they are responsible for all left-right communication, and presumably play a critical role in coordinating the proper phasing of flexor-extensor alternation between the two sides. Rhythmogenic interneurons are probably a heterogeneous group of interneurons which provide the rhythmic drive for the motor pattern. They have not yet been definitively identified, but since the fictive locomotor rhythm is generated from the lumbar region, then bursting activity should emanate from either a distinct subpopulation of neurons that burst endogenously, or from an as yet unspecified network of tonically active neurons which interact synaptically to generate the oscillatory drive for bursting. Ongoing and future anatomical, electrophysiological, and molecular genetic studies should further illuminate the subpopulation organization of the neuron types present in the CPG (Kullander 2005; Kiehn and Kullander 2004; Wilson et al. 2007).

Motoneurons are distributed throughout the spinal cord, with significant motoneuron pools driving flexor muscles located in L1 and L2, and motoneuron clusters driving extensor muscles in L5 and L6 (Kiehn et al. 2000). All cross-midline communication between hemicords is mediated by CINs (Puskár and Antal 1997), which may synapse onto MNs or other CINs, as well as other interneurons (Birinyi et al. 2003), and which are distinguished by the direction of their axonal projections (rostral, caudal, rostral and caudal, intrasegmental) (Eide et al. 1999; Stokke et al. 2002). CINs from each of the projective classes may be either excitatory or inhibitory. Though NMDA application can evoke

stable, locomotor-like rhythmic bursting in pharmacologically isolated motoneurons (Kjaerulff and Kiehn 2001), and 5-HT enhances CIN excitability (Zhong et al. 2006a, b), neither type of neuron appears to burst intrinsically *in vivo* .

As stated above, the composition of the rhythm generating component of the locomotor CPG is not known at present. A small percentage of ventromedially located, but otherwise unidentified, interneurons have been found to exhibit pacemaker-like burst oscillations when treated with neuromodulators (Hochman et al. 1994; Kiehn and Kjaerulff 1996), and some interneurons that express the HB9 homeodomain transcription factor, a genetic marker, burst rhythmically in the presence of 5-HT, NMDA, and DA (Wilson et al. 2005; Hinckley et al. 2005). The exact functions of the various oscillatory subpopulations remain unclear (Crone et al. 2008), but their bursts are consistent with fictive locomotion, and there is some evidence that they might form excitatory glutamatergic synaptic connections with motoneurons that are rhythmically active during fictive locomotion (Brownstone and Wilson 2008). The locomotor rhythm may be fundamentally a network oscillation, but it is possible that endogenously bursting interneurons also play a role in rhythmogenesis.

Real interneurons (CINs and RGNs) may be either excitatory or inhibitory, and they may act monosynaptically or via polysynaptic pathways, but in our CPG models we simplify connections as having functionally excitatory or functionally inhibitory effects. For example, two paths for cross-cord inhibition have been demonstrated experimentally: direct, monosynaptic CIN to contralateral MN inhibition, and indirect, polysynaptic CIN to contralateral MN inhibition via excitation of an intermediate interneuron (Butt and Kiehn 2003; Quinlan and Kiehn 2007). For modeling purposes, we treat both pathways as functionally equivalent (monosynaptic) CIN to contralateral MN inhibition.

The CPG models we consider here do not include feedback to the RGN neurons from the MNs, and CINs do not participate in rhythmogenesis. Though intrinsic currents may boost oscillations or contribute to postinhibitory rebound, phase relationships in the networks' output are largely independent of which membrane currents are present in the model MNs and CINs. In this paper, we do not focus on the intrinsic properties of the MN and CIN neurons, which may act primarily to amplify the effects of synaptic currents (Lee and Heckman 2000) stemming from RGN inputs. Instead we explore the functional implications of the strength and pattern of synaptic coupling.

1.3 Network organization and rhythmogenesis

Excitatory and inhibitory chemical synaptic connections are known to exist between various populations of CINs and MNs (Butt et al. 2002; Butt and Kiehn 2003; Birinyi et al. 2003), and at least excitatory connections are presumed to exist between RGNs and other CPG neurons, since rhythmogenesis continues in the presence of blockers of inhibitory synaptic transmission. The known inhibitory synaptic pathways involve $GABA_A$ and glycine (Butt and Kiehn 2003), while the excitatory synaptic pathways are glutamatergic (Kjaerulff and Kiehn 1997). In the neonatal spinal cord, localized groups of MNs show gap junction coupling (Kiehn et al. 2000; Tresch and Kiehn 2002), and there may be gap junctions between CINs and potential RGNs as well (Zhong et al. 2006a, b; Wilson et al. 2005).

There are cross-commissural synaptic connections throughout the lumbar and thoracic regions, involving both excitation and inhibition; there may be considerable redundancy in the organization of reciprocal inhibitory and excitatory connections in the CPG (Cowley and Schmidt 1997). Functionally speaking, intrasegmental communication between hemicords is largely inhibitory, implying that left-right alternation is mediated primarily through a combination of monosynaptic and polysynaptic inhibition (Kremer and Lev-Tov 1997; Butt and Kiehn 2003; Quinlan and Kiehn 2007). Intrasegmental and descending (from L2 to L5) intersegmental commissural synaptic pathways have been extensively mapped (Kjaerulff and Kiehn 1997; Bracci et al. 1997; Butt and Kiehn 2003), culminating in a broadly accepted and highly useful diagrammatic model of the CPG's organization (Fig. 1) (Butt and Kiehn 2003; Endo and Kiehn 2008; Kiehn 2006; Kiehn et al. 2008; Nishimaru et al. 2006; Quinlan and Kiehn 2007). The cross-cord connections in this model include contralateral extensor-extensor and flexor-flexor inhibition, as well as contralateral flexor-extensor and extensor-flexor excitation (Butt and Kiehn 2003). The output of the network's complicated mix of monosynaptic and polysynaptic inhibition and excitation cannot be captured by the diagrammatic model alone, however. Our understanding of the CPG's dynamic behavior may be significantly augmented by studying dynamic computational models, such as those presented in this paper.

The locomotor rhythm in the CPG appears to be generated predominantly by rostral portions of the lumbar spinal cord, propagating caudally, but the exact nature of the rhythmogenesis has not been conclusively determined through experiment. Multiple studies have found that interneurons in the L2 segment are active

during both flexor and extensor phases of the fictive locomotor rhythm (Cazalets et al. 1995, 1996; Butt and Kiehn 2003). The L4–L5 segments are also capable of independent rhythmogenic activity: experiments in which the spinal cord is divided transversely at L3 (via complete sectioning or Vaseline barriers in split-bath experiments) have demonstrated excitability to rhythmic bursting in both rostral and caudal segments (Beato and Nistri 1999; Cazalets and Bertrand 2000; Christie and Whelan 2005). Neuromodulator-induced oscillatory activity may differ between the rostral and caudal areas, depending on the neuromodulators used (Christie and Whelan 2005), and there appears to be a gradient of intrinsic rhythmic ability that is maximal in lower thoracic and upper lumbar segments and that weakens along the rostral-caudal axis (Tresch and Kiehn 1999). There is general consensus that locomotor rhythmogenesis emerges from (endogenous or network) bursting activity, and intra- and intersegmental synaptic connections coordinate and set the phasing of bursting activity to produce fictive locomotor patterns.

This scenario is compatible with coupled oscillator models, the approach taken in this paper. We assume that each network of neurons driving a group of extensor or flexor muscles is capable of generating an oscillatory output without input from the remainder of the network. This contrasts with traditional "half-center" models in which reciprocal inhibition of tonically spiking neurons results in bursting with an alternating rhythm. Endogenous oscillations of the right and left halves of the spinal cord have been observed to persist when the spinal cord is cut longitudinally (Kjaerulff and Kiehn 1996), supporting this hypothesis. There is general consensus among experimentalists that excitatory interneurons are the primary components of the rhythmogenic kernel, and that flexor-extensor alternation is coordinated in large part by a combination of monosynaptic and polysynaptic inhibition. The functional organization of our model reflects this arrangement, but represents groups of neurons as single cells and collapses polysynaptic pathways into functionally equivalent monosynaptic connections.

Our proposed architecture also accords with suggestions for modular organization of locomotor CPGs using "unit burst generators" (UBGs) as basic building blocks (Grillner 1981; Kiehn and Kjaerulff 1998). In this framework, UBGs capable of independent oscillation each control the activity of different synergistic muscle groups. Synaptic network connections coordinate the relative phases of the oscillators, but they are not necessary for the establishment of oscillations. The models studied here instantiate coupled oscillator models for

the RSHL CPG with bursting oscillators and synaptic coupling based on the information described above.

2 Computational models

The thrust of our current modeling study is to examine possible synaptic mechanisms that contribute to organizing the rhythmic alternation of bursts in the RSHL CPG. For simplicity, we use endogenously bursting cells to represent the oscillatory kernels in the CPG, and these RGNs are the only intrinsically oscillatory elements in our models. As previously stated, it is unknown whether rhythmogenesis in the biological CPG is produced by endogenous bursters, network-based oscillation, or both. We may thus view the RGNs as modeling burster involvement in rhythmogenesis or as a simplified way of modeling oscillatory subnetworks that normally produce rhythmic bursting. In both cases, a single cell model is used to represent the underlying oscillatory network. Under either interpretation of the RGNs in the model, we are able to focus on the effects of different configurations of synaptic coupling on the phasing of oscillatory elements in the CPG.

We use conductance-based, Hodgkin-Huxley-style model neurons with well-studied properties as components of our model network. In the absence of detailed information about the active conductances in different classes of spinal neurons, model cells with only a small number of active conductances are used. Our RGN model incorporates the minimum number of currents required for bursting (three dynamic variables evolving on different time-scales), and our MN and CIN model have the minimal intrinsic currents needed for tonic spiking capability. Along with speeding computations, these reductions remove any amplification of or interference with synaptic effects by the neurons' intrinsic currents, which simplifies our study of the effect of synaptic coupling in setting phase relationships between the oscillatory components. As more experimental information emerges regarding the various neuronal classes in the CPG, we can revise our neuron models to investigate the influence of specific intrinsic currents on the network's behavior.

Recognizing that they are necessarily incomplete representations of the real CPG, we have tried to strike a balance between biological realism and analyzability in building our models. Neither the models' synaptic connectivity nor single neuron representations incorporate all known biological features, but our models eschew the strong simplifying assumptions underlying the phase oscillator modeling approaches that are often used to study the role of CPGs' synaptic architectures

in gait patterning. Instead, we try to maintain enough biophysical and anatomical accuracy in the models' representations of the biological system to be able to relate (qualitatively or semi-quantitatively) our computational investigations to experiments. In a manner analogous to laboratory experiments where some (subsets of) cells are isolated from the rest of a preparation in order to isolate one or a few features, we study small networks to focus on the roles of particular subsets of synapses in patterning CPG output.

2.1 Full model

The full model comprises twelve neurons, four each of MNs, RGNs, and CINs. One neuron of each type represents the activity of corresponding networks of similar neurons in the (left or right) L2 (flexor) and L5 (extensor) segments of the spinal cord. The neurons are connected by sixty synapses (32 inhibitory, 28 excitatory); the network architecture of the model is best described by the wiring diagram in Fig. 1.

Neuronal models RGNs, MNs, and CINs are represented as single compartment, Hodgkin-Huxley-style model neurons, with equations as given in the Appendix and parameter values as listed in Table 1. The equations for all three neuron types were adapted from model I of Butera et al. (1999a), originally developed for respiratory neurons from the pre-Bötzinger complex of neonatal rats; we refer to this model with its original parameter values simply as the pre-Bötzinger model. Both the pre-Bötzinger model and the RGN model include a fast activating, slowly inactivating persistent sodium current, I_{NaP}, that helps set the baseline excitability of the cells and is the slow current responsible for bursting. The bursts are square-wave, or Type I, with spike frequency adaptation. Current injection increases the burst frequency while decreasing burst duration (Butera et al. 1999a); burst frequency and duty cycle can be controlled independently by adjusting the maximal persistent sodium conductance and the leak reversal potential (Tien 2007). The RGN model's endogenous burst characteristics (period, duty cycle, etc.) are listed in Table 2. We constrain our models
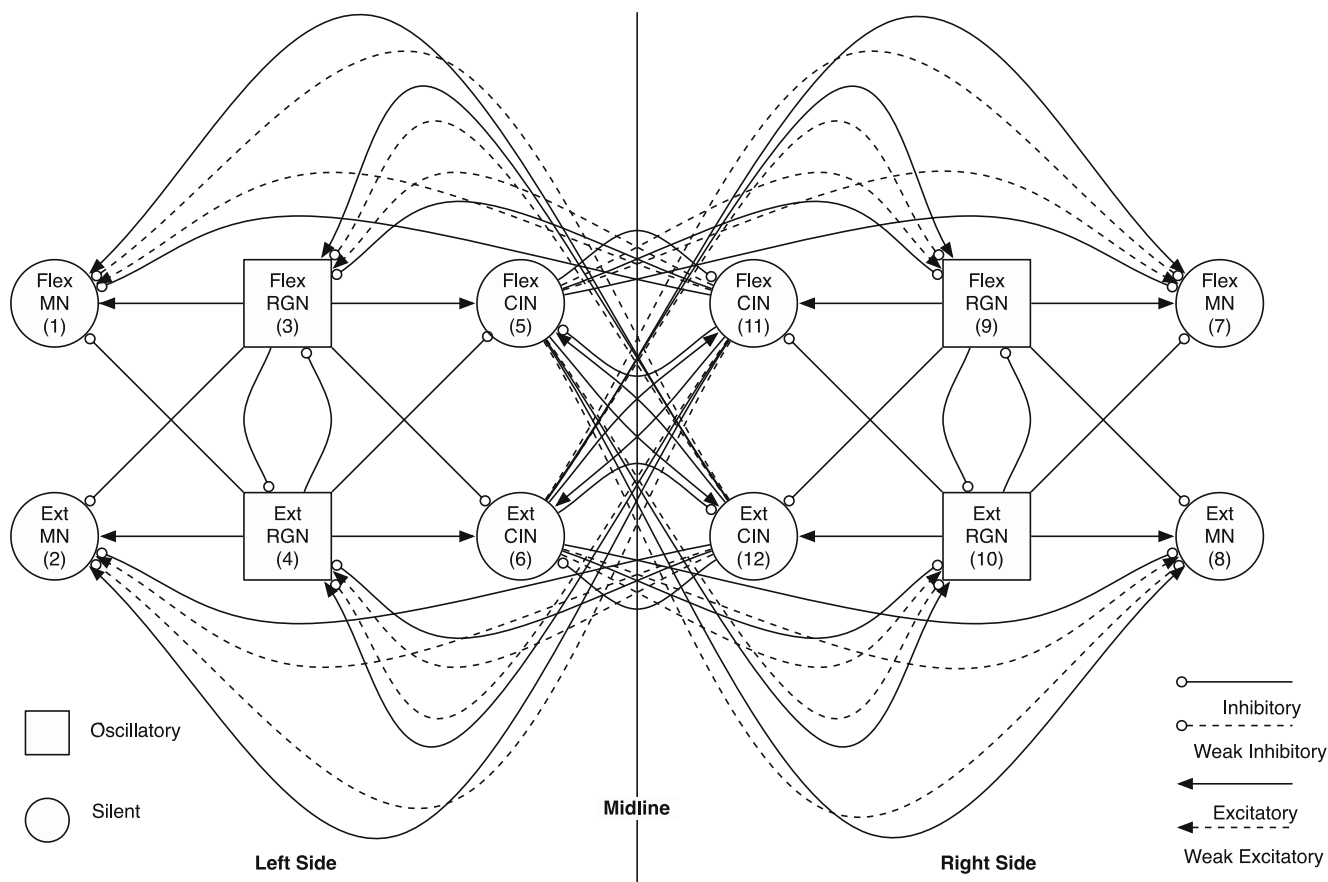

Fig. 1 Diagram of the full CPG model

Table 1 CPG neuron species parameter values

Parameter	CIN/MN	RGN
C	21	10
I_{app}	2	0
g_{Na}	45	28
V_{Na}	50	50
θ_m	−37	−34
k_m	−5	−5
g_{NaP}	–	3.3
V_{NaP}	–	50
$\theta_{m_{NaP}}$	–	−40
$k_{m_{NaP}}$	–	−6.3
θ_h	–	−47.89
k_h	–	9
$\overline{\tau}_h$	–	7,000
g_K	11.2	11.2
V_K	−85	−85
θ_n	−29	−29
k_n	−4	−3.6
$\overline{\tau}_n$	10	10
g_L	3.4	2.8
V_L	−50	−60.8

to parameter regimes with duty cycles of at least fifty percent, which is the appropriate range for walking gaits.

The persistent sodium current has been shown to partially underlie spike initiation in mouse spinal motoneurons (Kuo et al. 2006), it contributes to pacemaker-like voltage oscillations in Hb9 interneurons (Ziskand-Conhaim et al. 2008; Tazerart et al. 2008), and blockade of I_{NaP} may disrupt fictive locomotion (Tazerart et al. 2007). The prevailing interpretation of the currently available experimental data is that I_{NaP} plays a role in rhythmogenesis in the mouse spinal CPG, but there is not complete unanimity on this point. Given our ansatz that rhythm generation in the CPG may be modeled using endogenously bursting neurons, however, there are advantages to using I_{NaP} as the slow current underlying burst oscillations in the RGNs. It is consistent with several experimental results, and it accords with other models of the mammalian locomotor CPG (Rybak et al. 2006b). Furthermore, it enables us to use an established oscillator model with well-characterized burst dynamics (Butera et al. 1999a; Best et al. 2005; Izhikevich 2000) for our models of the net-

Table 2 RGN reference burst characteristics

Characteristic	Value
Period	2,309 ms
Duty cycle	0.5289
Spike number	28
Mean ISI	44.59 ms
Min ISI	28.34 ms
Max ISI	100.93 ms

work, allowing the effects of the synaptic connectivity be more interpretable.

MNs and CINs share a set of current balance equations that omit the I_{NaP} terms from the pre-Bötzinger model formulation. They are capable of tonic spiking, but not bursting, and are set to a parameter regime chosen so as to leave them passive but capable of being excited to spike repeatedly in response to small depolarizations. They act as conduits for the burst depolarizations from the RGNs, with their responses being modified by an array of synaptic inputs. We are aware that there are many more conductances that have been characterized in these neurons, but we opt for simplified neuronal models in order to focus more fully on the roles of the synaptic interactions in pattern formation.

Synaptic model A synapse model with continuously voltage-dependent neurotransmitter release (Destexhe et al. 1994, 1998) is used for both excitatory and inhibitory synapses. Model parameters are given in Table 3. In this synapse model's original formulation, parameters were chosen to match fast AMPA receptor kinetics; the synaptic activity profile is similar to the parameter set chosen for the CPG synapses. The model equations have the form:

$$I_{syn} = g_{syn}s(V - V_{syn}) \tag{1}$$

$$\dot{s} = \alpha_{syn} T_\infty(V_{pre})(1 - s) - \beta_{syn}s \tag{2}$$

$$T_\infty(V_{pre}) = (1 + \exp(-(V_{pre} - V_p)/K_p))^{-1} \tag{3}$$

Here s represents the level of neurotransmitter released into the synaptic cleft and thus actively affecting the post-synaptic cell. The neurotransmitter release rate is determined by Eq. (2), and depends on the presynaptic membrane voltage, V_{pre}, and the amount of neurotransmitter already released. The parameter K_p controls the sharpness of the change in the neurotransmitter release rate in response to changes in presynaptic voltage. Smaller K_p values produce rapid release, approximating spike-evoked synaptic transmission, while larger K_p values produce gradual release, resembling graded synaptic transmission. For our chosen K_p value, our models' synaptic activity is effectively spike-evoked.

The value of the synaptic reversal potential, V_{syn}, determines whether the synapse is excitatory or inhibitory; the parameter values match estimates of synaptic reversal potentials in the neonatal rat (Raastad et al. 1998). In all other respects (activation time constants, etc.) inhibitory and excitatory synapses are identical. The model synapses are non-adapting, as neither synaptic facilitation nor depression have yet been

Table 3 Synaptic parameters

Parameter	Description	Units	Value
g_{syn}	Maximum synaptic conductance	mS/cm^2	–
V_{syn}	Synaptic reversal potential	mV	−53 (inhibitory), 0 (excitatory)
α_{syn}	Open-closed transition rate	s^{-1}	2.162
β_{syn}	Closed-open transition rate	s^{-1}	0.2162
K_p	Transmitter voltage-response steepness	mV	4
V_p	Synaptic half-activation voltage	mV	−20

shown to play a strong role in information transfer in the RSHL CPG (Raastad et al. 1997).

2.2 Derived models

The full model is a dynamical system with 88 phase space variables and over 700 parameters. Even considering the symmetries of the model, the wiring diagram is complicated. Tracing the downstream phasing effects of some connections is not easy, and the size of the model makes numerical simulation computationally demanding. Brute-force exploration of the space of synaptic weightings for the full model is neither feasible nor likely to be particularly enlightening. To facilitate analysis and speed computations, we concentrate on two sets of subnetworks that have obvious functional importance for the operation of the full model. By studying the phasing characteristics of the derived models, we gain insight into the potential output repertoire and properties of the full model.

Two-cell models   The first set of subnetworks consists of two-cell models, both shown in Fig. 2(a): (1) 2-I, a pair of reciprocally inhibitory RGNs, and (2) 2-E, a

Fig. 2 Diagrams of reduced CPG models. Lines with *filled arrowheads* as endpoints indicate excitatory synaptic connections; lines with *open circles* as endpoints indicate inhibitory synaptic connections. (**a**) *Left*: rhythmogenic kernel (2-I), *right*: mutually excitatory pair (2-E). (**b**) Bi-directional inhibitory ring (4-IR). (**c**) Two half-center oscillators with cross-excitation (4-CE). (**d**) Bi-directional inhibitory ring with cross-excitation (4-IRCE)
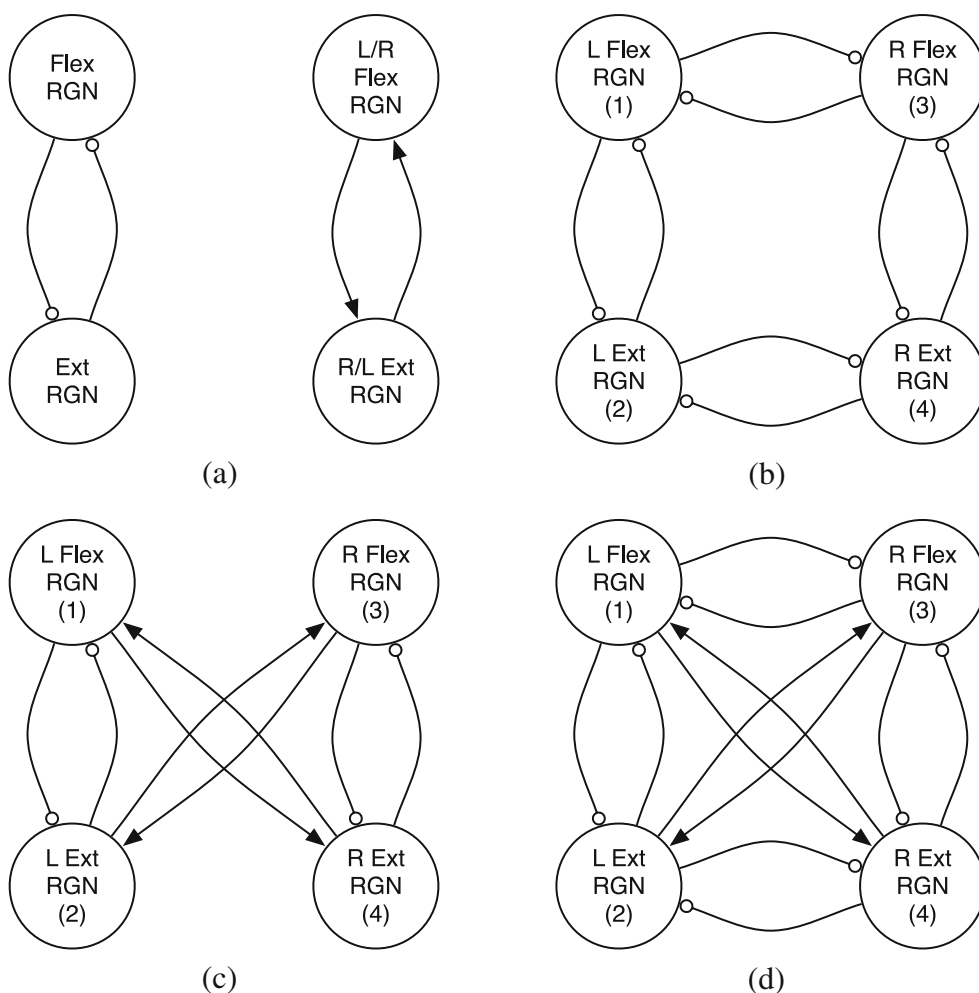
pair of mutually excitatory RGNs. 2-I is the two-cell rhythmogenic kernel present on each side of the full model, with each RGN reflecting the flexor or extensor rhythmogenic networks on that side. This is a variation on the usual half-center oscillator configuration, comprising two reciprocally inhibitory endogenous bursters rather than coupled tonically spiking neurons. Reduction to the 2-I model accords with the hypothesis that this subnetwork drives the rhythm of flexor-extensor alternation in each hemicord. The excitatory pair 2-E, not present in the full model, is a reduction of the excitatory cross-midline communication route that is mediated by CINs, collapsing the CINs together with the RGNs on each side. We use it to determine the range of excitation strengths that produce rapid synchronization of contralateral flexor-extensor pairs.

Four-cell models The second set of derived models consists of three four-cell networks, whose diagrams are shown in Fig. 2(b–d): (1) 4-IR, a bi-directional inhibitory ring of RGNs, (2) 4-CE, two half-center oscillators with cross-excitation between contralateral flexor and extensor RGNs, and (3) 4-IRCE, a bi-directional inhibitory ring of RGNs with cross-excitation. These networks are three plausible arrangements for coordinating flexor-extensor burst alternation across the midline in order to set up the fundamental locomotor rhythm. They may be considered reductions of the full model in which most of the excitatory connections have been removed and the MNs and CINs have been collapsed together with the RGNs. The resulting networks possess minimal sets of functional synaptic connections that (potentially) suffice to produce the fundamental walking rhythm robustly (cf. Figure 9 of Beato and Nistri 1999).

2.3 Model evaluation

We focus on three questions in testing our models: Is the phase configuration corresponding to the fundamental locomotor rhythm observed and stable? How quickly can the system establish the fundamental rhythm starting from a different, unorganized state? What are the phase resetting properties of the CPG model when the locomotor rhythm is interrupted and restarted?

The first question poses a minimal functional test of the aptness of our models as representations of the RSHL CPG. The isolated rodent spinal cord produces motoneuronal output resembling the fundamental locomotor rhythm when treated with certain neurotransmitters and other chemical agents, and neonatal rodents naturally develop the ability to crawl and walk. Hence we evaluate the capability of our models to produce the phase relationships required for the fundamental locomotor rhythm as their default behavior.

The second question is prompted in part by the behavior of the spinal CPG in whole-cord fictive locomotion experiments: the neuronal networks in the rodent spinal cord self-organize so as to stably produce walking-like patterns when activated (with neurotransmitters or electrical stimulation) from an unorganized state; switching from non-walking to walking states in the intact animal may occur similarly. Alternatively, the CPG in the intact animal may maintain itself in one of a number of pre-locomotor states ('idling') from which it can rapidly switch to locomotor activity; the CPG should then self-organize into one of these pre-locomotor configurations when starting from an unorganized state. Under either scenario the models should converge to fundamental locomotor rhythm from a wide range of initial conditions, possibly via a distinct sequence of intermediate, pre-locomotor configurations.

The third question investigates the ability of the models, once they have established the fundamental locomotor rhythm, to respond to fast changes in stimulation without extended transients, i.e. rapid recovery from perturbation. This is essential for escape behavior in the lamprey (Grillner 2003), for example, and this functional criterion has been used to rule out single component modulation as a mechanism for controlling burst frequency in models of the lamprey swimming CPG (Lansner et al. 1998).

We address these questions not only for the full model but also for each subnetwork model, testing several combinations of synaptic coupling strengths. Viewing the models from a dynamical systems perspective, each rhythmic locomotor pattern or gait (synchrony, hopping, walking, etc.) corresponds to a periodic orbit in phase space. The biologically motivated questions above may be recast in terms of the existence, stability, basin of attraction, and phase response properties of various periodic orbits of the models, with particular emphasis on the orbit associated with the fundamental locomotor rhythm. If the periodic orbit corresponding to a particular locomotor pattern exists and is stable in a given model, then the model's convergence to that periodic orbit from a point in phase space away from the orbit, i.e. a point representing an unorganized initial state or the model's state after perturbation from a stable locomotor pattern, is determined by the topography of the orbit's basin of attraction.

This last mathematical fact allows us to address all three of the questions above with computational

experiments that track the progression of the CPG models' phase configurations. The trajectories of the models (through phase configuration space), when started from a wide range of initial conditions, reveal the topography of the basin(s) of attraction of the models' stable phase configuration(s). If the fundamental locomotor rhythm is reproducible and stable for a given model, then the model will converge to it from many initial conditions (question one), and the rate at which the model converges from 'random' initial conditions directly reflects the system's ability to establish the fundamental locomotor rhythm when starting from unorganized initial states (question two). The third question may be investigated directly by starting the model in the fundamental locomotor rhythm, applying a perturbation at a particular phase of the locomotor cycle, and tracking the model's recovery to the fundamental locomotor rhythm. Much of the information that can be garnered from this direct approach, however, can also be inferred from the shape(s) of the basin(s) of attraction of the model's stable phase configuration(s): a perturbation that interrupts the fundamental locomotor rhythm effectively restarts the model from a different phase configuration which lies in the basin of attraction of (one of) the model's stable phase configuration(s). Thus from the shape(s) and convergence rate(s) of the model's basin(s) of attraction, we can infer the rates and target configurations following phase resetting perturbations of the fundamental locomotor rhythm.

We therefore study our models' behavior in regions of phase space (potentially) containing periodic orbits that correspond to various gaits, investigating their convergence and phasing behavior as synaptic strengths are systematically varied.

Target phase configurations In the full model, ipsilateral reciprocally inhibitory pairs of RGN cells are responsible for setting up the basic flexor-extensor alternation for each side, and thus we consider antiphasic alternation of flexor and extensor bursts (phase difference of 0.5) to be the target configuration of the 2-I subnetwork. Similarly, cross-cord excitation plays a role in synchronizing contralateral pairs of flexors and extensors, so that burst synchrony (phase difference 0) is the target configuration for the 2-E model. The four-cell (and full) models may possess several potentially stable phase configurations of biological interest, including complete synchrony, hopping, and walking. We prefer that walking be the most stable phase configuration of an RSHL CPG model, and consider that to be the target configuration of each four-cell model.

Coupling strength There is no clearly articulated standard by which modelers or experimentalists classify synaptic coupling as strong or weak. One measure of relative synaptic strength is the size of the maximal synaptic current in comparison to the strongest intrinsic current, typically the spiking sodium current. Other studies involving conductance-based neural models subjected to synaptic input (both excitatory and inhibitory) have used maximal synaptic currents whose ratios to the maximal spiking sodium current magnitude range from order 0.00001 to 1 (Acker et al. 2003; Nadim et al. 1995; Butera et al. 1999b; Prinz et al. 2003), classifying synaptic input strength as weak or strong in an apparently ad hoc fashion. Here we propose a more systematic terminology for synaptic coupling strength based on the ratio of maximal synaptic current to the maximal inward spiking current: Coupling with a ratio of order less than 0.01 is 'weak,' between 0.01 and 0.1 is 'intermediate,' and above 0.1 is 'strong.' Since the parameter g_{syn} is proportional to the ratio of maximal synaptic current to the maximal inward spiking current, we use g_{syn} as a convenient proxy for coupling strength in the remainder of this paper. For our models, $g_{syn} \leq 0.5$ provides effectively weak coupling, i.e. ratio to maximal $I_{Na} \leq O(0.01)$, and $g_{syn} \geq 5$ corresponds to effectively strong coupling.

Testing protocols For both two- and four-cell models, we assess their stable phase configurations and sensitivities to initial phasing conditions. We first consider a single uncoupled RGN cell evolving along the stable periodic orbit corresponding to its endogenous burst cycle. We term this periodic orbit the *individual reference orbit* or *individual reference burst*, and we choose the start of the active segment of the individual reference burst as reference phase 0. The initial conditions defining the individual reference orbit are given in Table 4.

For each two-cell network, we begin both of its neurons in an uncoupled state, i.e. $g_{syn} = 0$. We fix the initial conditions of one neuron, designated the 'leader,' at the point corresponding to reference phase 0. The initial conditions of the other neuron, designated the 'follower,' are set to correspond to a phase $\theta \in [0, 1]$. The synaptic strength is then set to its chosen value (coupling is symmetric), the synaptic activation

Table 4 Initial conditions for RGN reference burst trajectory

Phase variable	Value
V	−54.35234971337889
n	0.00087326528619
h	0.56373041060320

variables are initialized to 0, and the evolution of the two-cell model from this initial phase offset is simulated by numerically integrating for at least 15 burst cycles. The phase offset (relative phase) between the leader and follower neurons is calculated for the ith burst cycle as $(t_F^i - t_L^i)/T$ mod 1, where $t_{\{L,F\}}^i$ is the starting time of the ith burst of the leader or follower, respectively, and T is the period of the burst cycle.[2] For both the 2-I and 2-E networks, 50 evenly spaced initial follower phases $\theta \in [0, 1]$ were used as initial conditions. Coupling strengths g_{syn} ranged from 0.0001 to 40 for 2-I and from 0.00001 to 20 for 2-E.

We would expect the 2-I model to tend towards the antiphase configuration ($\theta_i \to 0.5$) and the 2-E model to tend towards synchrony ($\theta_i \to 0$). We considered a two-cell model to have functionally converged to a 'target' configuration if its Euclidean distance (in phase) to the target configuration shrank to less than 0.05 and remained within that bound for the duration of the simulation

For each four-cell model, we designate neuron 1 (corresponding to the left flexor) as the reference neuron against which all relative phases are measured. We fix the initial conditions of neuron 1 at reference phase 0, the start of the active segment of the individual reference burst. The initial conditions of the other neurons are set to correspond to random phases θ_i, $i = 2, 3, 4$, chosen uniformly in [0, 1]. The coupling strengths and synaptic variables are then initialized, and the model is simulated for at least 8 burst cycles. The phase offset $\Delta\theta_i^n$ of the ith neuron's nth burst is measured with respect to the nth burst of neuron 1, i.e. $\Delta\theta_i^n = (t_i^n - t_1^n)/T$ mod 1, where t_i^n is the starting time of the nth burst of cell i and T is measured as for the two-cell case.

The four-cell models' coupling architectures do not preclude them from producing the basic bipedal gaits (Pinto and Golubitsky 2006). However, precisely which gaits the different models preferentially produce cannot be determined by inspection of their wiring diagrams alone, divorced from the underlying dynamics of their oscillatory components. Potentially stable phase

configurations ('target' configurations) in our notation include:

1. complete synchrony: $\Delta\theta_i = 0, \forall i$
2. rhythmic left-right alternation: $\Delta\theta_3 = \Delta\theta_4 = 0.5$, $\Delta\theta_2 = 0$
3. hopping: $\Delta\theta_2 = \Delta\theta_4 = 0.5$, $\Delta\theta_3 = 0$
4. walking: $\Delta\theta_2 = \Delta\theta_3 = 0.5$, $\Delta\theta_4 = 0$
5. $^1/_4$-rotated: $\Delta\theta_2 = 0.25$, $\Delta\theta_3 = 0.5$, $\Delta\theta_4 = 0.75$

Configurations 1–4 correspond to activity patterns seen in whole-cord fictive locomotor experiments in neonatal rodents, translated into strict phase relationships constrained by the symmetries of the synaptic architectures. (Wider ranges of phasing, including asymmetries and overlaps in flexor-extensor activation, are possible during various locomotor gaits and postures in intact and decerebrate animals (Pearson and Rossignol 1991; Yakovenko et al. 2005); greater symmetry in flexor-extensor activation patterns is seen in other fictive locomotion experiments (Kiehn and Kjaerulff 1996, 1998; Kiehn et al. 2000; Kiehn and Butt 2003). In isolated spinal cord experiments in rodents, where sensory feedback is removed, the measured duty cycles for flexor and extensor motoneuron activity are both close to 50% (Butt et al. 2002).) Configuration 5 has no biological counterpart in this context, but its appearance would serve to indicate a failure of the CPG model to produce biologically relevant output.

Each model was simulated starting from 100 random initial phase configurations for each set of inhibition and/or excitation strengths. We calculated the Euclidean distance from the various target configurations listed above for each of the 100 trajectories at each burst cycle. For a given initial phase configuration, if the model's distance to a target configuration shrank to less than 0.15 (which would be achieved with a phase difference of 0.05 for each neuron, for example) and remained within that bound for the duration of the simulation, the model was said to have converged to that target configuration. The mean and variance of the population distance to the different target configurations are useful indicators of the models' global convergence behavior. The proportion of simulations that evolve to phasing arrangements near a given configuration is indicative of the size of the target configuration's basin of attraction; the rate of accumulation reflects both the stability of the target phase configuration and the influence of the chosen synaptic strength.

Inhibitory g_{syn} values were 0.001, 0.01, 0.1, 1, 5, 10, 15, 20; excitatory g_{syn} values were 0.0001, 0.001, 0.01, 0.1, 1, 5. For some simulations of the 4-IR and 4-IRCE models, ipsilateral and contralateral inhibitory

---

[2]For the networks examined in this paper, the period of the burst cycle of each coupled RGN stabilized within a few cycles (typically fewer than four) to a value close (within 0.1–5%) to the period of the uncoupled RGN burst cycle, regardless of whether the phase differences between component neurons converged. The period T here can be taken as the period of the individual (uncoupled) reference burst or as the (stable) period of the coupled burst without any qualitative difference in the results, and only a very slight quantitative difference in the measured phase offsets. The results in the next section use the coupled burst period.

g_{syn} values were the same (symmetric inhibition), while for other simulations ipsilateral and contralateral inhibition were different (asymmetric inhibition).

Except for locating periodic orbits, we performed all calculations with PyDSTool, a software package written in C and Python for the simulation and analysis of dynamical systems (Clewley et al. 2007). The integration routine was a fifth-order variable-time step implicit method with eighth-order dense output (Radau5, Hairer and Wanner 1991) for stiff systems, with relative and absolute error tolerances of 10^{-10} for both solvers. Phenomena of interest, such as spike peaks or the onset of the actively spiking segment of the burst cycle, were detected during integration by testing for zero crossings of appropriately defined event functions at each time step. Using the integrator's dense output and a bisection method, these were located to within an accuracy of 10^{-8}. The individual reference orbit was found using multiple shooting with automatic differentiation (Guckenheimer and Meloon 2000), as implemented in the ADMC++ automatic differentiation package for MATLAB (Phipps 2003), with error less than 10^{-12}.

3 Results

3.1 Full model

We simulated the full CPG model under many combinations of inhibitory and excitatory coupling strengths for many initial conditions, but we did not exhaustively search the (high dimensional) space of plausible synaptic weights. The computational costs incurred by such a survey would be prohibitive, while the volume of data collected would pose significant organizational and interpretive challenges. We chose instead to begin exploring the synaptic weight space of the full CPG model interactively, systematically varying the strengths of synapse groups that intuition suggested should play leading roles in setting the relative phasing of the CPG output, i.e. MN bursts. These synapse groups included, for example, reciprocal inhibition between ipsilateral flexor and extensor RGNs, and contralateral excitation from CINs to RGNs of a different type. Though the strengths of the various synapse groups changed relative to one another, cross-midline and rostral-caudal (flexor-extensor) symmetry in synaptic coupling was maintained.

Partial output from a typical simulation of the full CPG model is presented in Fig. 3 (simulations were usually run for 10–20 burst cycles). In this example, there is initially approximately 50% overlap between the active phases of the flexor and extensor RGNs on

each side, while each flexor RGN begins roughly out of phase with the contralateral extensor RGN. That is, the initial phasing is the opposite of the proper walking pattern. Within three burst cycles, however, simultaneous ipsilateral flexor-extensor alternation and cross-cord flexor-extensor synchronization have been established, and this fundamental locomotor rhythm is henceforth stably maintained. The transition to the walking configuration is effected through the elongation of the active segments of both flexor RGNs and the simultaneous shortening of the active segments of both extensor RGNs during the first two cycles. The pattern of this transient period, namely changes in the durations of overlapping active segments for some subset of RGNs, is typical of trajectories of the full model that ultimately lead to the fundamental walking rhythm. Every combination of RGNs whose burst durations transiently vary is possible, depending on the initial phasing conditions and the exact set of synaptic strengths. In our simulations, spike timing and the duration of the active spiking segment of RGN bursts typically varied up to 50% and in some cases more than doubled, but the RGN interburst interval showed much less variability (5–15%). Once the model settled into a stable phase configuration, whether synchronous or alternating, the intraburst and interburst intervals also stabilized, with minimal overlap between opposing RGNs' active segments.

Note that the output from the CINs and MNs shown in Fig. 3 follows the bursting pattern and phasing of their respective driving RGNs almost perfectly, with the CINs and MNs firing spike for spike with the RGNs. This activity pattern held for a wide range of (contralateral and ipsilateral) CIN-CIN and CIN-MN coupling strengths. By reducing the strength of excitatory coupling from their driving RGNs, the CINs and MNs could be driven to fire once every two or three RGN action potentials; this had no effect on the phasing of MN/CIN bursts relative to the RGNs. Neither inhibitory nor excitatory cross-cord synaptic connections from CINs to MNs (respectively, CINs) had any noticeable effect on the phasing of MN (CIN) bursts (relative to the bursts of the MNs' (CINs') driving RGNs), but intermediate-strong excitatory CIN-MN (CIN-CIN) synaptic connections could change spike timing and spike number within MN (CIN) bursts.

It is common for a computational model to be presented as successfully reproducing the behavior of a given biological system with little accompanying discussion of how tightly the model's parameters must be tuned in order to obtain appropriate output. Figure 3 shows "correct" output from the CPG model, in that the system does eventually reproduce the fundamental
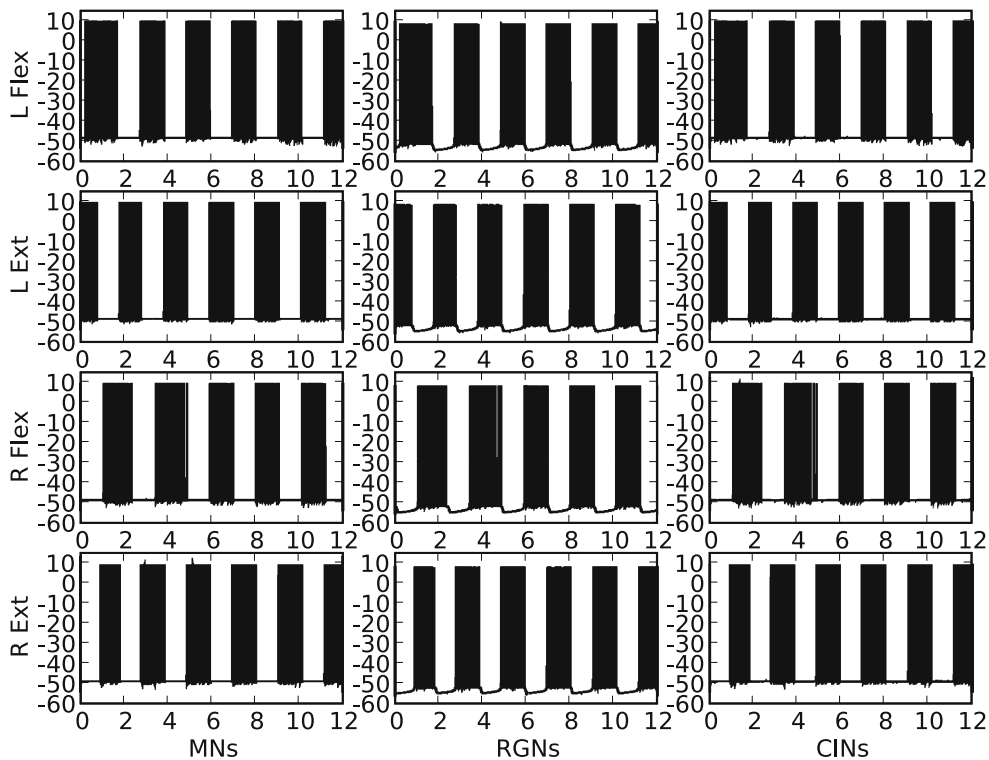
Fig. 3 Sample output of the full CPG model. The y-axes record membrane voltage in mV; the x-axes record time in seconds. Output from neurons associated with left or right flexor or extensor output are organized along the rows. Columns are organized by neuron type. In this example, the initial RGN phasing was $\Delta\theta_2 = 0.3$, $\Delta\theta_3 = 0.65$, $\Delta\theta_4 = 0.71$ mod 1, taking the left flexor RGN as neuron 1. Synaptic coupling strengths were 0 except: ipsilateral RGN-MN and RGN-CIN flexor-extensor inhibitory $g_{syn} = 5$ (synapses {(3, 2), (4, 1), (9, 8), (10, 7)}, {(3, 6), (4, 5), (9, 12), (10, 11)}), ipsilateral RGN-RGN inhibitory $g_{syn} = 20$ (synapses {(3, 4), (4, 3), (9, 10), (10, 9)}), contralateral CIN-CIN and CIN-RGN inhibitory $g_{syn} = 5$ (synapses {(5, 11), (11, 5), (6, 12), (12, 6)}, {(5, 9), (11, 3), (6, 10), (12, 4)}), ipsilateral RGN-CIN and RGN-MN excitatory $g_{syn} = 40$ (synapses {(3, 5), (4, 6), (9, 11), (10, 12)}, {(3, 1), (4, 2), (9, 7), (10, 8)}), contralateral CIN-RGN excitatory $g_{syn} = 0.01$ (synapses {(5, 9), (11, 3), (6, 10), (12, 4)})

locomotor rhythm. From the fifth burst cycle onwards, the relative phasing of MN (and CIN and RGN) bursts differs by less than 0.5% from the configuration we denoted as walking in the previous section. Achieving this behavior required significant tuning of the synaptic weights, and deviation from a relatively sensitive balance of coupling strengths for some apparently critical sets of synapses either dramatically slowed the model's convergence to the fundamental locomotor rhythm or destroyed convergence entirely. Table 5 reports the synaptic strength ranges for which the model reliably converged to the fundamental locomotor rhythm, and it summarizes the rough organization of the synapses into distinct groups according to their heuristic roles in establishing and/or modulating convergence to the walking mode.

Twenty 'critical inhibitory synapses,' comprising five functional groups, required relatively high g_{syn} values in order for the fundamental locomotor rhythm to be produced reliably. Twelve of these synapses act primarily to promote ipsilateral flexor-extensor alternation; in particular, the minimum strength of reciprocal inhibition between ipsilateral RGNs was quite high ($g_{syn} \geq 15$). For the minimum strengths listed for ipsilateral critical inhibitory connections, without compensatory excitation, contralateral CIN-CIN and CIN-RGN inhibitory $g_{syn} \geq 5$ were lower bounds for cross-cord inhibition. Thus all of the critical inhibitory synapses must be functionally strong for the normal locomotor pattern to emerge. Though the overall level of inhibition in the full CPG model could be doubled, the g_{syn} ratios between the sets of inhibitory synapses had to remain within a relatively narrow range. That is, from a given combination of inhibitory synaptic weights such that the full model rapidly and reliably produced the fundamental locomotor rhythm, varying the g_{syn} value for any one set of inhibitory synapses by more than approximately ±10% typically destroyed or slowed the model's convergence to the walking configuration. The strength of ipsilateral RGN-RGN inhibition was an exception: for a given 'successful' synaptic weighting, ipsilateral RGN-RGN inhibition could typically be doubled or

Table 5 Roles of different synapse groups in establishing the fundamental locomotor rhythm in the full model

Role	Functional group	Synapses	Strengths	Effect(s)
Conduit synapses	Ipsilateral RGN-MN excitation	(3, 1), (4, 2), (9, 7), (10, 8)	$2 \leq g_{syn} \leq 10$	–
	Ipsilateral RGN-CIN excitation	(3, 5), (4, 6), (9, 11), (10, 12)	$2 \leq g_{syn} \leq 10$	–
	Ipsilateral RGN-RGN F-E inhibition	(3, 4), (4, 3), (9, 10), (10, 9)	$g_{syn} \geq 15$	⋆
Critical inhibitory synapses	Ipsilateral RGN-MN F-E inhibition	(3, 2), (4, 1), (9, 8), (10, 7)	$g_{syn} \geq 5$	⋆
	Ipsilateral RGN-CIN F-E inhibition	(3, 6), (4, 5), (9, 12), (10, 11)	$g_{syn} \geq 5$	⋆
	Contralateral CIN-CIN inhibition	(5, 11), (11, 5), (6, 12), (12, 6)	$g_{syn} \geq 5$	⋆
	Contralateral CIN-RGN inhibition	(5, 9), (11, 3), (6, 10), (12, 4)	$g_{syn} \geq 5$	⋆
Modulatory excitatory synapses	Contralateral CIN-RGN F-E excitation	(5, 10), (11, 4), (6, 9), (12, 3)	$0.5 \leq g_{syn} \leq 2$	↑
	Contralateral CIN-CIN F-E excitation	(5, 12), (12, 5), (6, 11), (11, 6)	$g_{syn} \geq 0.1$	↑↓
	Contralateral CIN-RGN (weak) excitation	(5, 9), (11, 3), (6, 10), (12, 4)	$g_{syn} \geq 0.01$	↓
	Contralateral CIN-MN inhibition	(5, 7), (11, 1), (6, 8), (12, 2)	–	–
Relatively ineffectual synapses	Contralateral CIN-MN F-E excitation	(5, 8), (11, 2), (6, 7), (12, 1)	–	–
	Contralateral CIN-RGN F-E (weak) inhibition	(5, 10), (11, 4), (6, 9), (12, 3)	–	–
	Contralateral CIN-MN F-E (weak) inhibition	(5, 8), (11, 2), (6, 7), (12, 1)	–	–
	Contralateral CIN-MN (weak) excitation	(5, 7), (11, 1), (6, 8), (12, 2)	–	–

Effects of synapses with strengths in the given ranges are indicated by various symbols: (⋆) approximate lower bounds for convergence; (↑) faster convergence; (↓) slower/disrupted convergence; (—) minimal effect on convergence

tripled without adversely affecting the convergence of the model to the fundamental locomotor rhythm. Except for the value given for ipsilateral RGN-RGN inhibition, the strengths of the inhibitory synapses for the example shown in Fig. 3 reflect the lowest g_{syn} values of the critical inhibitory synapses that were required to produce the fundamental locomotor rhythm reliably.

For a given set of inhibitory synaptic weights, several combinations of excitatory synaptic strengths typically led to the walking configuration, but the convergence behavior of the model was often particularly sensitive to changes in the amount of excitation. Varying the strength of a few key excitatory connections by ±10% could slow or destroy convergence to walking, but which excitatory connections were 'key' and what effects they had depended on the configuration of the other inhibitory and excitatory synaptic weights. Almost always, however, the strengths of the 'modulatory excitatory synapses' greatly affected the convergence behavior of the model. In particular, contralateral CIN-RGN flexor-extensor/extensor-flexor excitation, within rather narrow bounds, increased the rate of convergence to the walking configuration (to within 2–3 burst cycles), while any contralateral extensor-extensor or flexor-flexor CIN-RGN excitation of moderate or greater strength tended to disrupt the fundamental locomotor rhythm significantly. Contralateral CIN-CIN excitatory $g_{syn} \geq 0.1$ could either enhance or impair convergence to walking, depending on the values of other synaptic weights.

The strength of excitatory 'conduit synapses' connecting RGNs to ipsilateral MNs and CINs, once above the threshold to stimulate MN (respectively, CIN) spiking in response to RGN activity, had no effect on the phasing of CPG output. The lower values of the ranges given in Table 5 for these synapses record the minimum strengths such that RGN bursts stimulated MN/CIN bursts, and the upper values indicate the maximum strengths used in simulations of the full CPG model.

The remaining synapses, some of which one would expect to be rather weak, based on biological intuition, were 'relatively ineffectual,' i.e. altering their strengths elicited little change in the output of the model. With contralateral flexor-extensor/extensor-flexor CIN-MN connections, for example, so long as the critical inhibitory synapse strengths were above the minimum g_{syn} values listed in Table 5, neither excitation nor inhibition with $g_{syn} \leq 10$ had any noticeable effect on the model's behavior. Contralateral CIN-RGN flexor-extensor/extensor-flexor inhibition was similarly ineffectual. As reflected in Table 5, there was no range of strengths for which the relatively ineffectual synapses appeared to have much, if any, importance for convergence to or maintenance of the fundamental locomotor rhythm, relative to the critical inhibitory or modulatory excitatory synapses.

Though we did not simulate all combinations of synaptic strengths, our exploration of the synaptic weight space for the full CPG model leads us to make two heuristic observations regarding coupling strength and oscillator phasing.

First, the strength of reciprocal inhibition between ipsilateral flexor and extensor RGNs was the primary determinant of the speed with which each side converged into flexor-extensor alternation, with strong inhibition ($g_{syn} \geq 15$) being necessary to achieve alternation rapidly (within 2–3 burst cycles). The relative phasing of ipsilateral flexor and extensor output tended

to drift without strong reciprocal inhibition between the flexor and extensor RGNs. With weak to moderate reciprocal inhibition, flexor-extensor alternation might be achieved after six or more burst cycles, or not at all, depending on initial conditions. For a given level of reciprocal inhibition, excitatory inputs to the RGNs from contralateral CINs (flexor-flexor/extensor-extensor) could disrupt the flexor-extensor alternation, depending on the phasing of the contralateral flexor-extensor pair.

Second, both strong ipsilateral reciprocal inhibition and strong contralateral inhibitory and excitatory synaptic coupling onto the appropriate RGNs were needed in order to establish the fundamental locomotor rhythm within 2–3 burst cycles. Without strong ipsilateral reciprocal inhibition, there could be cross-cord synchrony (either extensor-extensor or flexor-extensor) without ipsilateral flexor-extensor alternation. Lack of cross-cord excitation typically led either to independent flexor-extensor alternation on each side (without fixed phasing between sides), or occasionally to hopping activity, with the latter more likely with stronger cross-cord inhibition onto RGNs.

In general, for a given set of synaptic weights, some initial conditions led the model to settle rapidly into a steady pattern, such as synchrony or the fundamental locomotor rhythm, while others did not. The stronger the overall level of synaptic coupling, the more likely the model was to converge to a fixed pattern and the more rapidly it did so.

These heuristic insights into the influence of various synapse groups on phasing support our architectural choices in deriving two-cell and four-cell reduced models. We used the two- and four-cell models to examine systematically the phasing roles of critical sets of synapses, as well as to investigate more thoroughly some unexpected behaviors of the full CPG model, such as its parametric fragility, the need for strong coupling, and non-monotonic cycle-to-cycle variability in phasing, intraburst and interburst intervals. With the 2-I and 2-E models (Section 3.2) we specifically investigate the phenomena of our first heuristic observation by focusing on RGN-RGN interactions in isolation and testing phasing behaviors as synaptic strength and initial conditions are varied. To better understand the second heuristic observation, we use the various four cell models to explore in greater detail the roles of connections representing the 'critical inhibitory' and 'modulatory excitatory' synapses of the full model (Section 3.3). Both the two- and four-cell model studies below bear on the general observation that stronger synaptic coupling correlated positively with more rapid convergence.

3.2 Two-cell models

Figure 4 shows the evolution of relative phase in the 2-I model of two mutually inhibitory RGNs for six representative coupling strengths. The θ_0-axis represents the initial follower phases, and the vertical θ_n-axis displays the follower phases (relative to the leader) after n burst cycles. Instantaneous convergence to antiphase would produce the horizontal plane given by $\theta_n = 0.5$, while the uncoupled system would produce 45-degree sloped plane given by $\theta_n = \theta_0$. Figure 5 shows the evolution of relative phase in the 2-E model of two mutually excitatory RGNs for six representative coupling strengths; the axes are the same as for the 2-I model.

2-I model For coupling strengths below 1, the 2-I model did not achieve the antiphase configuration from any initial conditions in less than 20 burst cycles; for coupling strengths greater than 20, every initial condition led to the antiphase configuration within three cycles, and most within two. None of the higher coupling strengths tested achieved the antiphase configuration within one cycle from every initial condition. As seen in Fig. 4, $g_{syn} = 20$ is approximately the lowest coupling strength for which the transient period is short enough for the model to meet our biologically motivated expectations of "rapid" phase resetting. The broad flat region at the $\theta_n = 0.5$ height in Fig. 4(f) indicates that from 70% of initial conditions θ_0, including most of the interval (0.2,0.8), the 2-I model with $g_{syn} = 20$ settled into the antiphase configuration within 4 burst cycles ($|\theta_n - 0.5| \leq 0.005$ and $|\theta_j - \theta_{j+1}| \leq 0.002, \ j \geq 4$). Every initial condition led to the antiphase configuration within 8 burst cycles. Very similar convergence behavior ($|\theta_n - 0.5| \leq 0.01$ and $|\theta_j - \theta_{j+1}| \leq 0.006, \ j \geq 4$) occurred for $g_{syn} = 15$ (Fig. 4(e)), but at this strength not every initial condition led to antiphase even after 10 burst cycles.

For lower coupling strengths, the convergence to the antiphase configuration from many initial conditions is so slow that the model could be considered as not having a functionally stable antiphase configuration at all, though initial conditions in a small region about $\phi_0 = 0.5$ do converge to within antiphase after a few burst cycles. This region of reasonably rapid convergence grows with increasing coupling strength.

When the neurons coupled in the 2-I configuration did settle into the antiphase configuration, their active spiking segments had up to two fewer spikes and their duty cycles were at most six percent shorter than for the reference orbit for the single uncoupled RGN. Weak coupling left the period for a complete oscillation essentially unchanged from that of the uncoupled reference orbit; at the strongest levels of coupling, the period

Fig. 4 Evolution of the relative phasing of bursts in 2-I model (half-center configuration) over eight burst cycles, for a variety of synaptic coupling strengths. The follower neuron's initial relative phase is recorded on the θ_0-axis; the follower neuron's relative phase after burst cycle n is indicated by height on the θ_n-axis
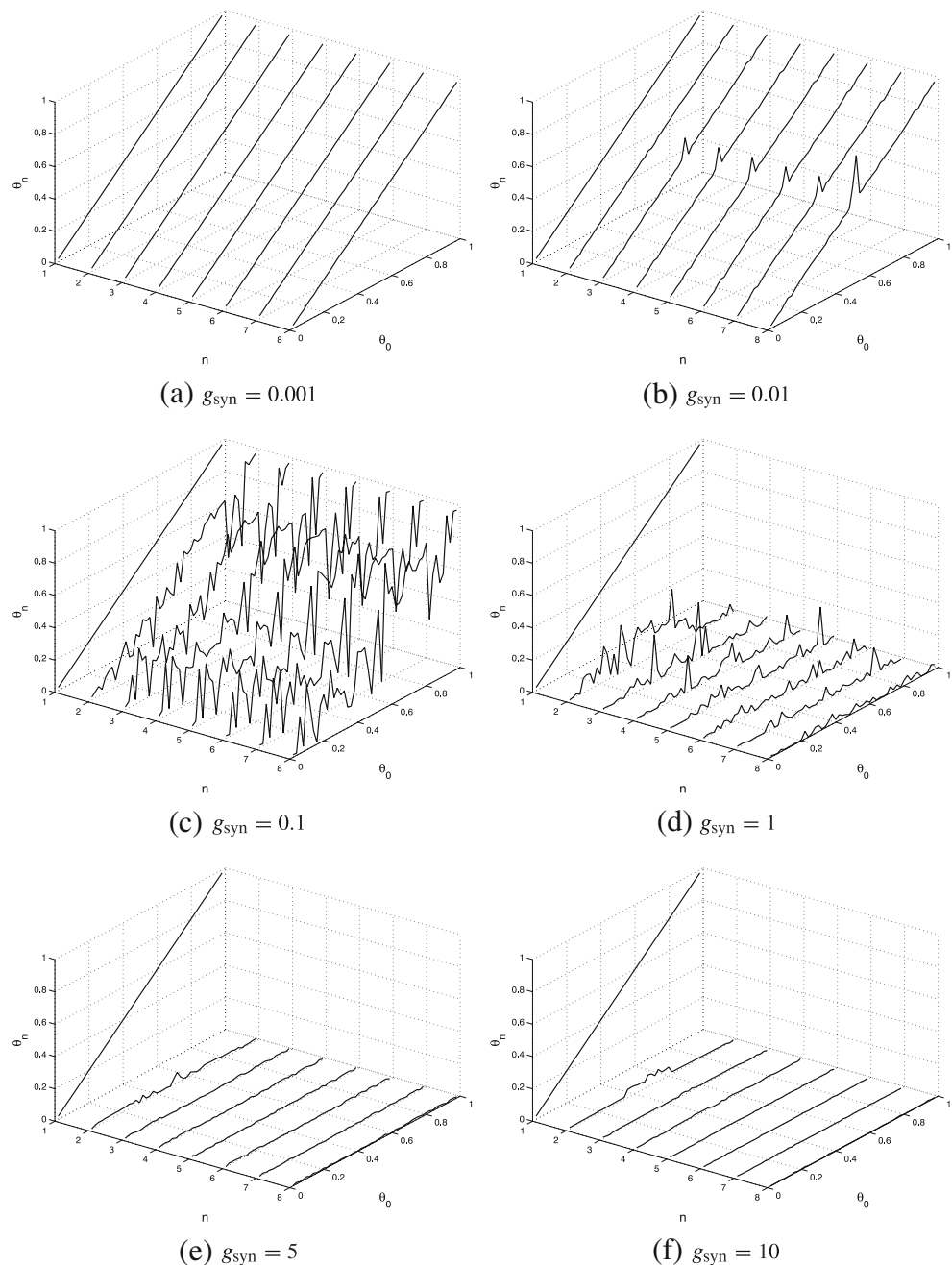
(a) $g_{syn} = 0.1$

(b) $g_{syn} = 1$

(c) $g_{syn} = 5$

(d) $g_{syn} = 10$

(e) $g_{syn} = 15$

(f) $g_{syn} = 20$
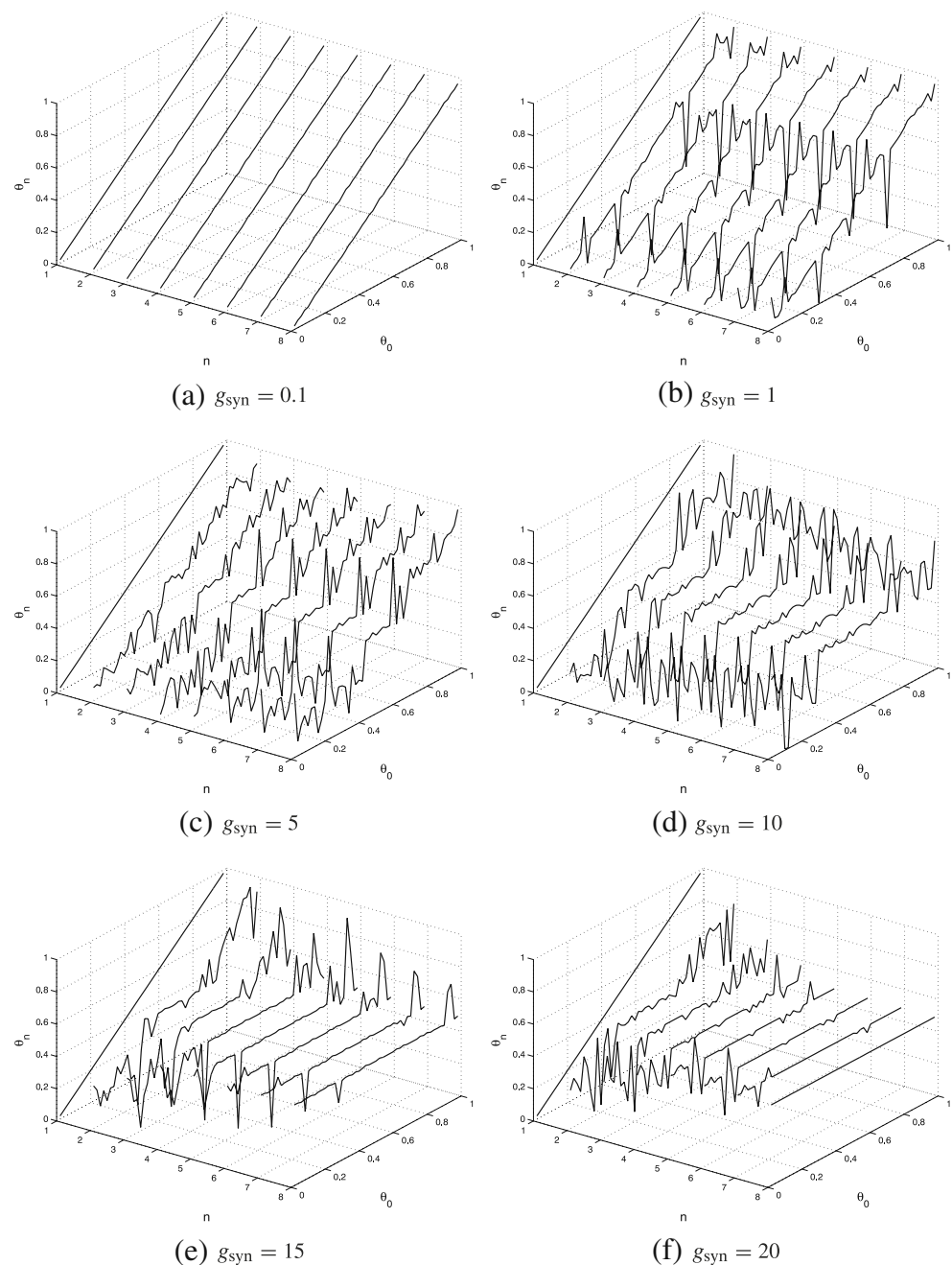
was reduced by at most five percent. In a sense, the neurons in the half-center configuration settle onto coupled periodic orbits that lie near their uncoupled starting orbits, but which minimize the amount of overlap between them, thus shrinking their duty cycles and reducing their spike numbers.

2-E model For coupling strengths below $g_{syn} = 1$, the 2-E model neurons did not synchronize their bursts for at least 15 cycles (Fig. 5(a–c)), while for strengths equal to or greater than $g_{syn} = 1$, bursts synchronized within 8 cycles (Fig. 5(d–f)). Biologically reasonable

synchronization rates (within 2–3 cycles) were achieved only for strengths 5 and higher. If we compare the magnitude of the synaptic currents to the magnitude of I_{Na}, as for the 2-I model, relatively strong coupling is required to achieve rapid burst synchrony in the 2-E model, but weaker than in the 2-I model.

We note that the neurons of the 2-E model typically settle into configurations of burst synchrony with intraburst spike anti-synchrony, a phenomenon previously reported in models of bursting in pancreatic β-cells (Sherman 1994) and in the pre-Bötzinger model (Best et al. 2005). The spikes of the two neurons

Fig. 5 Evolution of the relative phasing of bursts in 2-E model (half-center configuration) over eight burst cycles, for a variety of synaptic coupling strengths. The follower neuron's initial relative phase is recorded on the θ_0-axis; the follower neuron's relative phase after burst cycle n is indicated by height on the θ_n-axis

(a) $g_{\mathrm{syn}} = 0.001$

(b) $g_{\mathrm{syn}} = 0.01$

(c) $g_{\mathrm{syn}} = 0.1$

(d) $g_{\mathrm{syn}} = 1$

(e) $g_{\mathrm{syn}} = 5$

(f) $g_{\mathrm{syn}} = 10$

alternate, but their burst envelopes (defined by the activity of I_{NaP}) are almost completely synchronous. The alternation of spikes within synchronized bursts probably has little biological significance in terms of synchronization of flexor and extensor contraction.

Transient behavior and phase sensitivity The 2-I model displays a higher degree of sensitivity to initial phasing conditions than the 2-E model. As can be seen at higher coupling strengths in Fig. 4, the relative phases of the neurons may change significantly from cycle to cycle in a fashion that does not converge monotoni-

cally to a phase difference of 0.5: as the number of cycles n increases, the 45-degree line in Fig. 4(b–f) does not transform smoothly to a horizontal line; the pictures are instead quite jagged. This sensitivity to initial phasing conditions manifests itself in the transient behavior of the 2-I model as it moves towards its target configuration; in particular, the position of leader and follower may reverse one or more times before achieving antiphase (not shown). At the highest coupling strengths, this sensitivity diminishes for initial conditions about $\theta_0 = 0.5$, hence a flatter interval of the relative phasing curve emerges about this phase,

reflecting the neurons' rapid movement towards antiphase from nearby initial conditions. This flatter interval broadens as the coupling strength increases, but phase sensitivity remains for initial phases closer to 0 or 1.

Unlike the 2-I model, the 2-E model does not exhibit such significant sensitivity to initial phasing conditions, nor does it appear to manifest leader-follower switching behavior. For coupling strengths above $g_{syn} = 0.1$, all initial conditions eventually lead to synchrony, and nearby initial conditions typically synchronize by moving the bursts in the same direction. As can be seen in Fig. 5(d–f), the rate of synchronization is slower for initial conditions near antiphase (solid line peaks near $\theta_0 = 0.5$). These initial conditions correspond to the alignment of one neuron's active segment with the other's quiescent segment, and the slower convergence reflects the weaker phase response of the bursting neuron while it is inactive. We have investigated the mechanisms underlying this phenomenon and other aspects of phase response in endogenously bursting neural models (Sherwood 2008), and we report our findings in another paper (Sherwood and Guckenheimer 2009).

3.3 Four-cell models

We present our four-cell model simulation results in three-dimensional plots. The plots' axes measure the relative phases of the models' neurons with respect to the phase of reference neuron 1: the x-axis measures $\Delta\theta_2 = \theta_2 - \theta_1$ mod 1, the y-axis measures $\Delta\theta_3$, and the z-axis measures $\Delta\theta_4$. Inset beside each three-dimensional plot are projections of the three-dimensional data onto two dimensions. Projections onto the $(\Delta\theta_2, \Delta\theta_3)$-, $(\Delta\theta_2, \Delta\theta_4)$-, and $(\Delta\theta_3, \Delta\theta_4)$-planes are presented in the top, middle, and bottom two-dimensional inset plots, respectively. To help the reader interpret the plots, the diagram in Fig. 6 shows the location of relevant locomotor phase configurations in three dimensions and in two-dimensional projections.

Though phase is a circular variable, the three-dimensional plots are cubiform. One must imagine that the endpoints 0 and 1 of an axis are identified as a single point, with the measured phase differences 'wrapping around' at the endpoints. Thus plot markers near 0 and 1, though presented visually as being far apart, are in fact close together in phase. Figure 7(d) shows an example of such an artifact: there appear to be two distinct clusters of markers, but because $\Delta\theta_3 = 0$ is equivalent to $\Delta\theta_3 = 1$, the opposite faces of the $\Delta\theta_2 \times \Delta\theta_3 \times \Delta\theta_4$ cube of the plot are identified as one, and there is in fact a single cluster. Similar considerations apply to the two-dimensional projections: though the presentation is planar, these projections are in fact toroidal, so that their top and bottom edges are identified with one another, as are their left and right edges. Phase coordinates wrap around the top edge to restart at the bottom edge, and

Fig. 6 Locations of four-cell models' possible stable phase configurations. The *top*, *middle*, and *bottom* two-dimensional insets are projections of the three-dimensional figure onto the (θ_2, θ_3)-, (θ_2, θ_4)-, and (θ_3, θ_4)-planes, respectively. *Blue circles*: complete synchrony, $\Delta\theta_i = 0, \forall i$; *red diamonds*: rhythmic left-right alternation, $\Delta\theta_3 = \Delta\theta_4 = 0.5, \Delta\theta_2 = 0$; *green triangles*: hopping, $\Delta\theta_2 = \Delta\theta_4 = 0.5, \Delta\theta_3 = 0$; *black squares*: walking, $\Delta\theta_2 = \Delta\theta_3 = 0.5, \Delta\theta_4 = 0$; *magenta crosses*: $1/4$-rotated, $\Delta\theta_2 = 0.25, \Delta\theta_3 = 0.5, \Delta\theta_4 = 0.75$. *Solid* and *dashed connecting lines* are for visual orientation

(a) $g_{syn} = 0.1$

(b) $g_{syn} = 5$

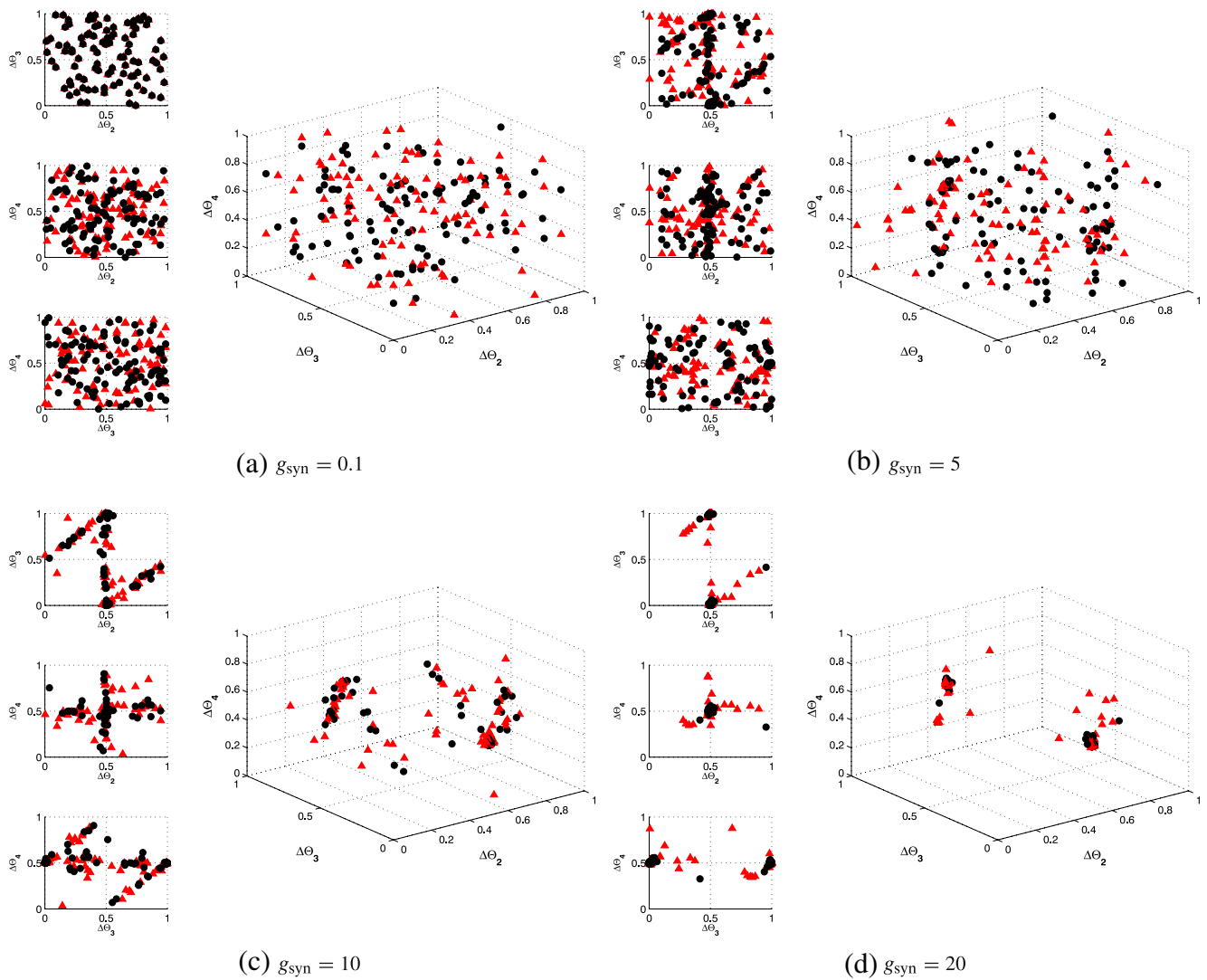(c) $g_{syn} = 10$

(d) $g_{syn} = 20$
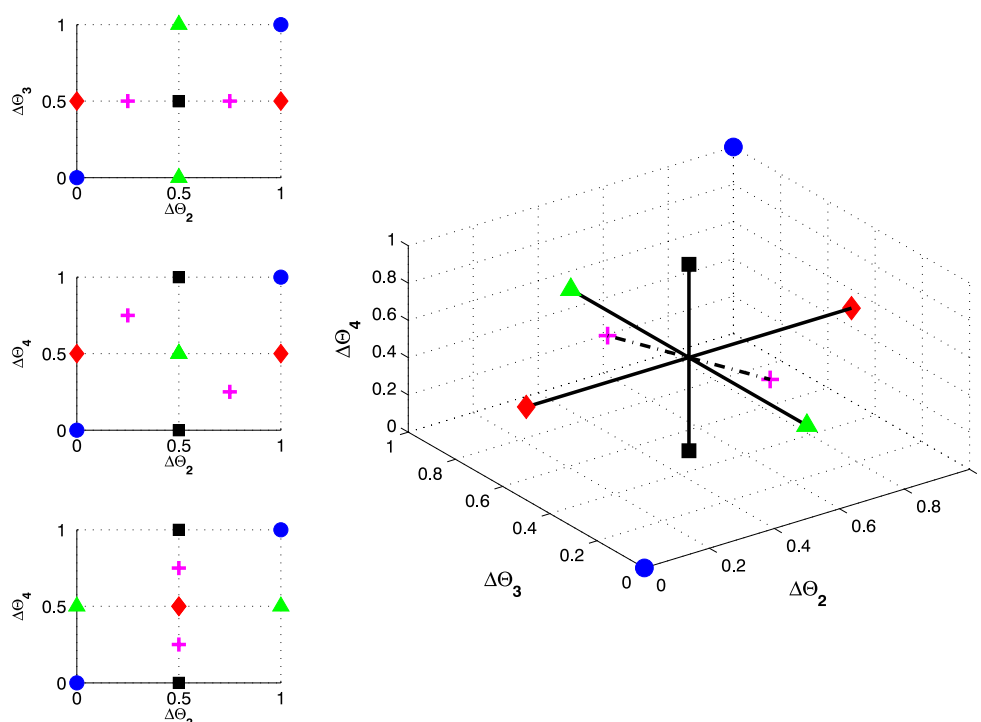
Fig. 7 Relative phasing of bursts in the 4-IR model for various strengths of symmetric inhibitory coupling, starting from 100 random initial phase configurations. *Red triangles* indicate phasing after three burst cycles; *black circles* indicate phasing after eight burst cycles

they wrap around the right edge to restart at the left edge. The two seemingly distinct clusters of Fig. 7(d) that also appear in the corresponding two-dimensional projections are, again, a single cluster.

Marker color and shape indicate the temporal progression of the simulations. Marking each simulation's relative phasing at every burst cycle produces cluttered, difficult to decipher figures, and so we plot relative phasing only at third and eighth burst cycles, using red triangles and black circles, respectively. Clustering of markers with the same shape/color (in particular, black circles) about a given phase point indicates that the model converges to the corresponding relative phase configuration. The size, shape, and distribution of marker shape/color for a cluster are related to the size and shape of its corresponding phase configuration's

basin of attraction and to the rate at which the model converges to that phase configuration from initial conditions within the basin of attraction.

For example, Figs. 11(f) and 13(c) both show marker clustering about $\Delta\theta_2 = \Delta\theta_3 = 0.5$, $\Delta\theta_4 = 0$; this single cluster (in terms of phase configuration) appears as two clusters at the centers of the top and bottom faces of the cubiform plots. The relative dearth of markers away from $\Delta\theta_2 = \Delta\theta_3 = 0.5$, $\Delta\theta_4 = 0$ indicates that there is a single attractive phase configuration in both plots. Convergence to the attractor is more rapid for Fig. 11(f), which has a tighter, smaller diameter cluster, than for Fig. 13(c), which has more widely dispersed red triangle markers (corresponding to earlier burst times in the simulations). 'Trails' of markers, such as those visible in Figs. 11(e) and 13(e), indicate the typical

trajectories (sequences of phase configurations) that the models traverse as they approach their final phase configurations.

In addition to the three-dimensional plots, for each model instance (combination of inhibition and/or excitation strengths) we graph the mean and variance of the Euclidean distance of the 100 simulations from the complete synchrony, hopping and walking target configurations at each burst cycle. The shapes of these graphs indicate the models' global convergence behavior; the slopes reflect the rapidity of convergence, and the variances may (indirectly) reflect the relative attractiveness of different target configurations and the sizes of their basins of attraction. In each of the mean Euclidean distance plots, the threshold for convergence to a given target configuration, i.e. a Euclidean distance of 0.15, is indicated with a horizontal dashed black line.

3.3.1 4-IR model

Symmetric inhibition From most initial conditions, symmetric inhibition (equal g_{syn} values for all contralateral and ipsilateral inhibitory synapses) weaker than $g_{syn} = 1$ produced practically no change in cell phasing for the 4-IR model, even after eight burst cycles. This can be inferred from graphs of mean distance to synchrony, walking, and hopping (Fig. 8), all of which are essentially static, with unchanging variance. In addition, the even distribution of phase configurations and the close proximity of the members of the red and black sets of markers in Fig. 7(a) indicate that the neurons' relative phases change very little over the course of the simulations.

At intermediate to strong levels of symmetric inhibition, there is much more movement, and some clustering emerges after 5 or more cycles. Some red and many black markers clump together near $\Delta\theta_2 = 0.5$, $\Delta\theta_4 = 0.5$, $\Delta\theta_3 = 0$, the 'hopping' configuration. This clustering is most prominent at $g_{syn} = 20$; the emergence of the hopping configuration is evident after three cycles in Fig. 7(d). The mean distance to the hopping configuration decreases monotonically, at a faster rate for higher levels of inhibition, as seen in Fig. 8. Only at the highest inhibition levels, however, does the variance in distance to hopping decrease significantly along with the mean. These results indicate that symmetric inhibition alone moves the network towards its stable configurations rather slowly, and at a biologically reasonable rate only for strong coupling strengths.

Surprisingly, the most attractive stable configuration available to the symmetric inhibitory ring network is not walking, but hopping, as seen in Fig. 8 and the substantial clustering of black and red markers in Fig. 7(b–d) near $\Delta\theta_2 = 0.5$, $\Delta\theta_4 = 0.5$, $\Delta\theta_3 = 0$ (the centers of the rear-left and front-right faces of the cubiform plot), but not elsewhere. The 4-IR model did not converge to the walking mode in any of our simulations, indicating that it is either unstable or its basin of attraction is vanishingly small. Complete synchrony among the oscillators is possible for the symmetric 4-IR model, but its basin of attraction is very tiny (not shown). The $^1/_4$-rotated configuration, in which each oscillator maintains a quarter-cycle offset from its neighbors, is completely absent, even though the network's symmetries imply that it should be an accessible phase configuration.

Asymmetric inhibition The preferred phase configurations of the asymmetric 4-IR model, in which $g_{syn}^{i,i}$ (ipsilateral reciprocal inhibition) and $g_{syn}^{i,c}$ (contralateral reciprocal inhibition) values are varied separately, differ from those for the 4-IR model with symmetric inhibition. As in the symmetric 4-IR model, $g_{syn}^{i,i}$ and $g_{syn}^{i,c}$ less than 1 resulted in very little change in cell phasing after eight burst cycles or more. At higher levels of inhibition, e.g. $g_{syn}^{i,i} \geq 5$, $g_{syn}^{i,c} \geq 5$, under conditions where contralateral inhibition was stronger than ipsilateral inhibition, the relative phases of the 4-IR model's neurons aligned along the line $\Delta\theta_3 \approx 0.5 \mod 1$, $\Delta\theta_2 - \Delta\theta_4 \approx 0.5 \mod 1$. Since the phase differences are measured with respect to neuron 1, these relations imply that the neurons within each contralateral pair (1 and 3, 2 and 4) were antisynchronized, but the relative phases within each ipsilateral pair (1 and 2, 3 and 4) were approximately uniformly distributed between 0 and 1. Thus the model preferred phase configurations intermediate between rhythmic left-right alternation and walking, as seen in Fig. 9(a). When overall inhibition was relatively high, but ipsilateral inhibition was stronger than contralateral inhibition, the relative phases aligned along the line $\Delta\theta_2 \approx 0.5 \mod 1$, $\Delta\theta_3 - \Delta\theta_4 \approx 0.5 \mod 1$ (intermediate between hopping and walking), as shown in Fig. 9(b).

Very strong ipsilateral inhibition in combination with even stronger contralateral inhibition, i.e. $g_{syn}^{i,i} \geq 20$, $g_{syn}^{i,c} \geq 30$, eventually produced convergence to the walking configuration from nearly every initial phasing condition. (The symmetric 4-IR model converged to the hopping configuration with comparable celerity for $g_{syn} = 10$.) As illustrated in Figs. 9(c) and 10, the neurons first assume relative phases that approximate rhythmic left-right alternation, then converge to the walking mode along the line $\Delta\theta_3 \approx 0.5 \mod 1$, $\Delta\theta_2 - \Delta\theta_4 \approx 0.5 \mod 1$. The model converged to walking

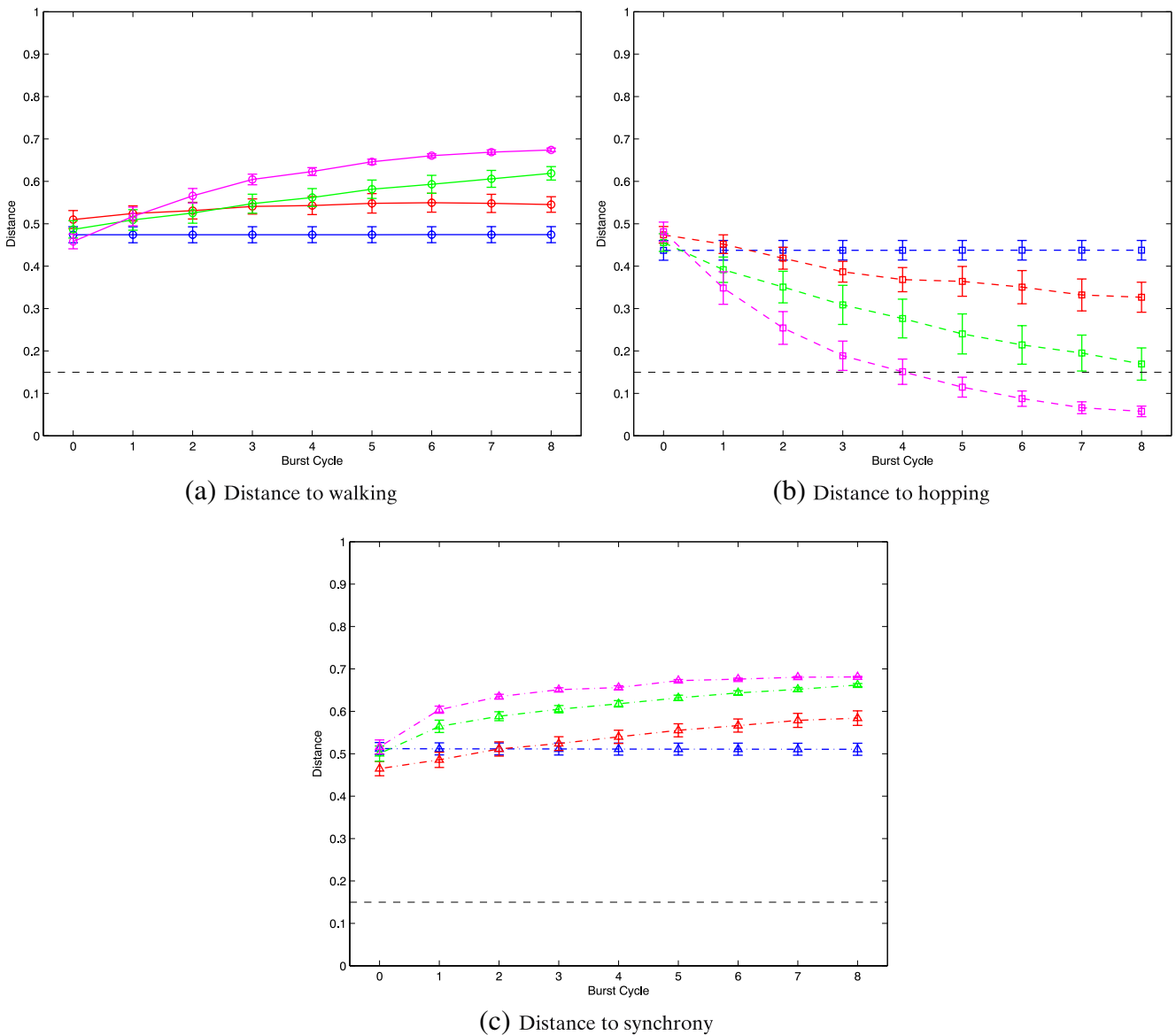(a) Distance to walking

(b) Distance to hopping

(c) Distance to synchrony

Fig. 8 Mean distance to target phasing configurations—(**a**) walking, (**b**) hopping, (**c**) synchrony—after each burst cycle in simulations of the 4-IR model for various strengths of symmetric inhibitory coupling. The *horizontal dashed black line* indicates the threshold for convergence to the target configuration. *Error bars* indicate variance; line color indicates coupling strength. (1) *Blue*: $g_{syn} = 0.1$. (2) *Red*: $g_{syn} = 5$. (3) *Green*: $g_{syn} = 10$. (4) *Magenta*: $g_{syn} = 20$

from most initial conditions within eight burst cycles, though a small number of simulations ($\approx 5\%$) took longer to move away from the hopping configuration. When contralateral inhibition was at least twice the strength of ipsilateral inhibition, i.e. $g_{syn}^{i,i} \geq 20$, $g_{syn}^{i,c} \geq 40$, the model reached the walking configuration within 2–3 burst cycles. With the right balance of very strong inhibition, the model converges to the appropriate gait pattern with biologically reasonable speed; excitation is not necessary to produce the fundamental locomotor rhythm.

3.3.2 4-CE and 4-IRCE models

Symmetric inhibition At every combination of g_{syn}^i (inhibition) and g_{syn}^e (excitation) values, the convergence behavior of the 4-CE and 4-IRCE model (which adds intrasegmental inhibition across the midline) was essentially identical when ipsilateral inhibition and contralateral inhibition were equal in the 4-IRCE model. We show figures only for the 4-CE model, since the corresponding figures for the symmetric 4-IRCE model were virtually indistinguishable, making their
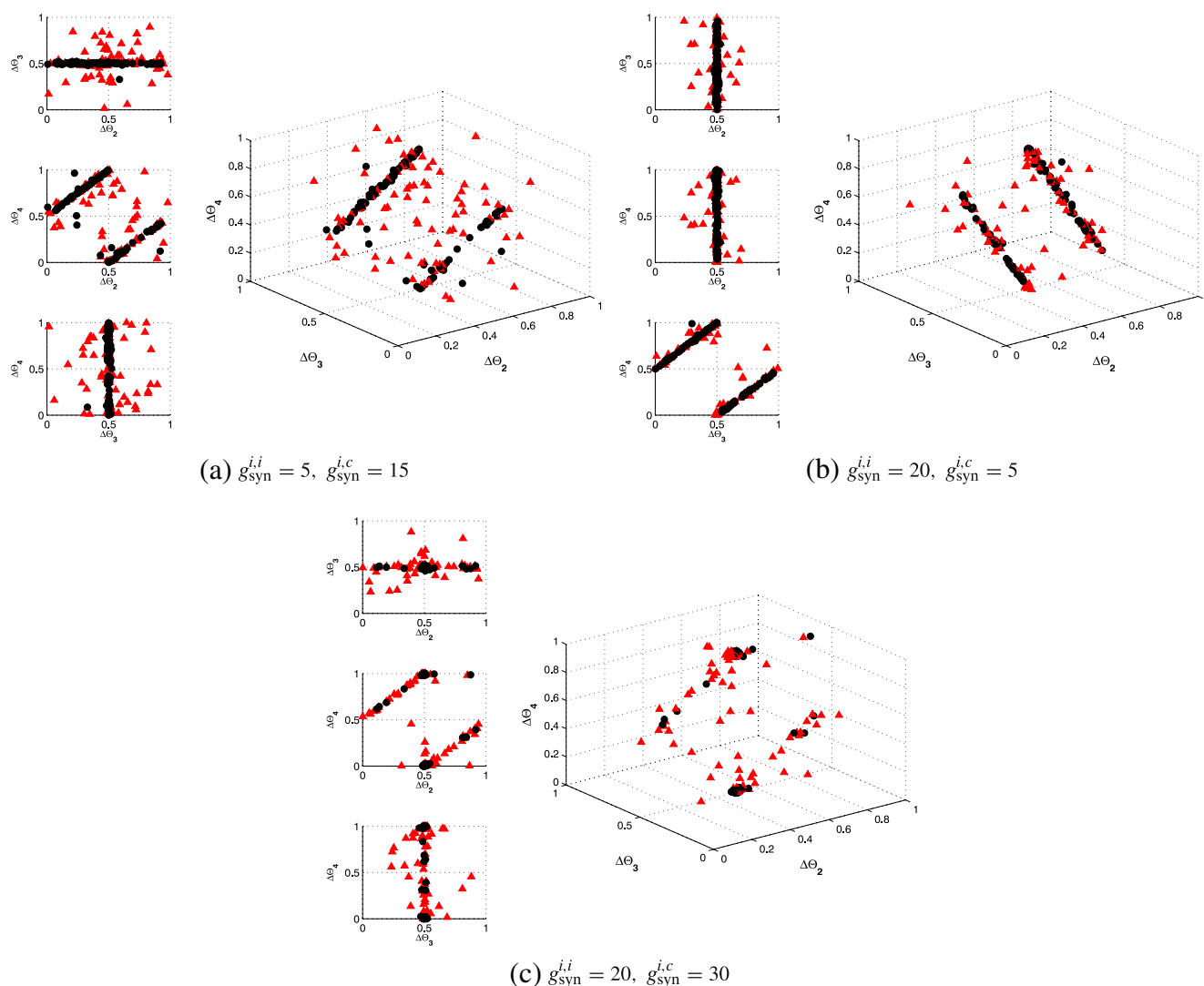
(a) $g_{syn}^{i,i} = 5$, $g_{syn}^{i,c} = 15$

(b) $g_{syn}^{i,i} = 20$, $g_{syn}^{i,c} = 5$

(c) $g_{syn}^{i,i} = 20$, $g_{syn}^{i,c} = 30$

Fig. 9 Relative phasing of bursts in the 4-IR model with separately varying levels of ipsilateral and contralateral inhibition, starting from 100 random initial phase configurations. *Red trian-gles* indicate phasing after three burst cycles; *black circles* indicate phasing after eight burst cycles

presentation redundant. The close similitude of the results for the 4-CE and symmetric 4-IRCE models indicates that the extra (cross-midline) inhibition present in the symmetric 4-IRCE model has no noticeable effect on phasing behavior.

For given values of g_{syn}^i and g_{syn}^e, the two models had convergence behaviors similar to those of the 2-I and 2-E models at the same levels of inhibition and excitation. That is, the rate of convergence to synchrony in excitatorily coupled pairs in the four-cell networks were similar to that of the 2-E model for a given g_{syn}^e value; the analogous statement for the convergence of inhibitorily coupled pairs was also true. For both models, excitation below $g_{syn}^e = 1$ and inhibition below $g_{syn}^i = 10$ were effectively weak in terms of achieving bi-

ologically reasonable convergence rates, though these g_{syn} values are intermediate to strong according to the standard introduced in Section 2.3. Such weak phase resetting behavior in response to strong perturbation resembles that seen in the 2-I, 2-E, and 4-IR models (cf. Figs. 4(a–c), 5(a–c); and 7(a)).

At the lowest levels of g_{syn}^i and g_{syn}^e, the relative phases of the models' neurons after many cycles remained essentially unchanged from their initial phasing; the results resembled Fig. 7(a) for the symmetric 4-IR model. Weak to intermediate (symmetric) inhibition and weak excitation produced movement in the relative phasing of the models' neurons, and the mean distance to the walking configuration declined slowly, but without a significant concomitant rise in the mean
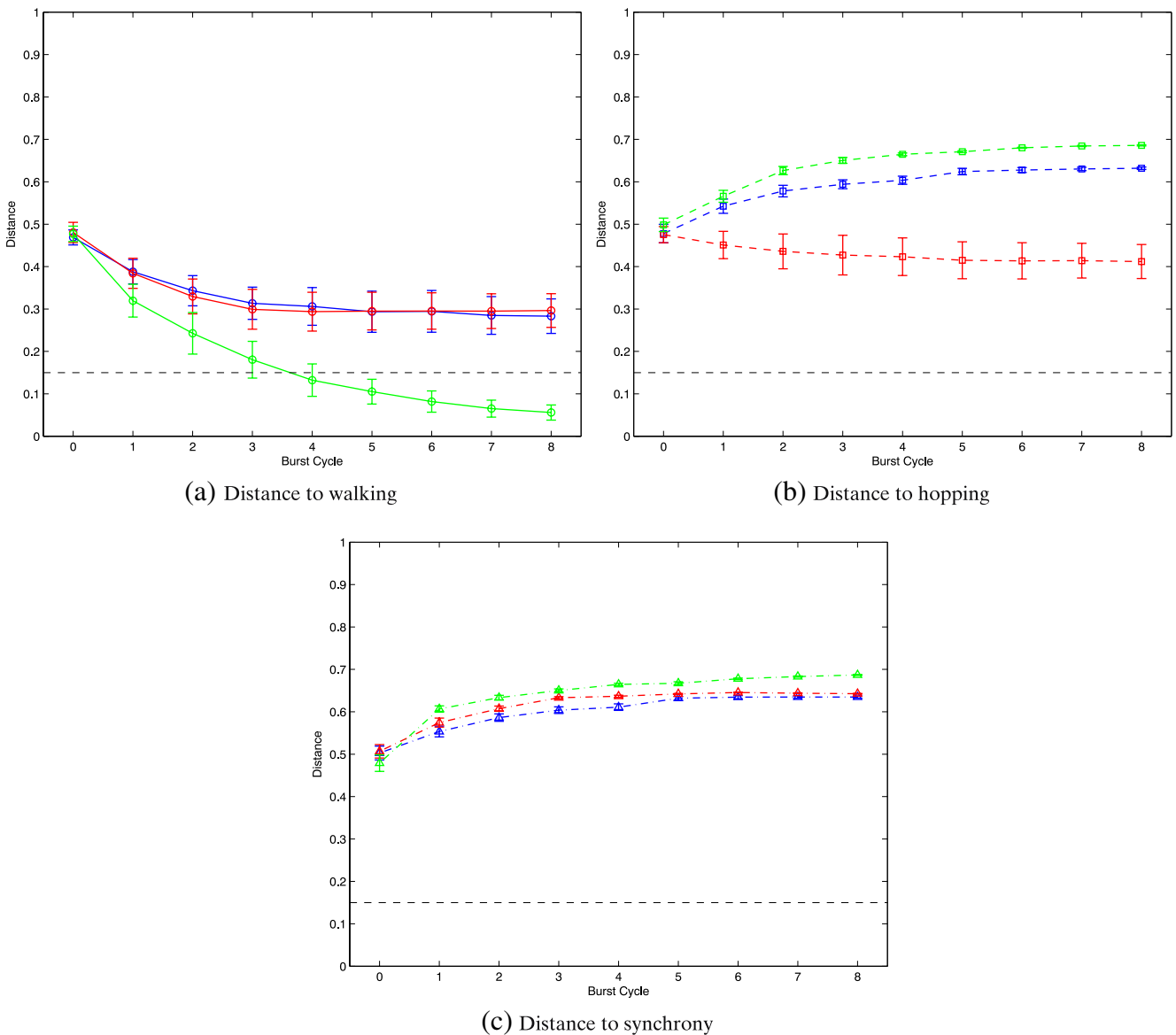
(a) Distance to walking

(b) Distance to hopping

(c) Distance to synchrony

Fig. 10 Mean distance to target phasing configurations—
(**a**) walking, (**b**) hopping, (**c**) synchrony—after each burst cycle
in simulations of the 4-IR model with separately varying levels
of ipsilateral and contralateral inhibition. The *horizontal dashed*

black line indicates the threshold for convergence to the target
configuration. *Error bars* indicate variance; line color indicates
coupling strength. (1) *Blue*: $g_{syn}^{i,i} = 5$, $g_{syn}^{i,c} = 15$. (2) *Red*: $g_{syn}^{i,i} = 20$, $g_{syn}^{i,c} = 5$. (3) *Green*: $g_{syn}^{i,i} = 20$, $g_{syn}^{i,c} = 30$

distance to hopping and synchrony, indicating no con-
vergence to a fixed phase configuration even after many
cycles (Figs. 11(a) and 12).

For intermediate to strong inhibition, if excita-
tion is increased to intermediate levels, e.g. $g_{syn}^i = 1, 5$; $g_{syn}^e = 1$ (Fig. 11(b)), the models converge fairly
rapidly to contralateral flexor-extensor synchrony. The
models' neurons' phases align along the line $\Delta\theta_4 \approx 0$
mod 1, $\Delta\theta_2 \approx \Delta\theta_3$ mod 1. That is, neurons 1 and 4
are synchronized, and 2 and 3 are synchronized, but
the relative phases between the {1, 4} pair and the

{2, 3} pair are uniformly distributed between 0 and
1. Similar, but tighter and more rapid, alignment oc-
curs for moderately strong symmetric inhibition and
excitation ($g_{syn}^i = 5$, $g_{syn}^e = 5$, Fig. 11(c)). The imme-
diate alignment along the contralateral flexor-extensor
synchrony axis is reflected in the evolution of mean
distance to target configurations, shown in Fig. 12:
distance to synchrony initially drops substantially, then
rises, while distance to walking declines gradually and
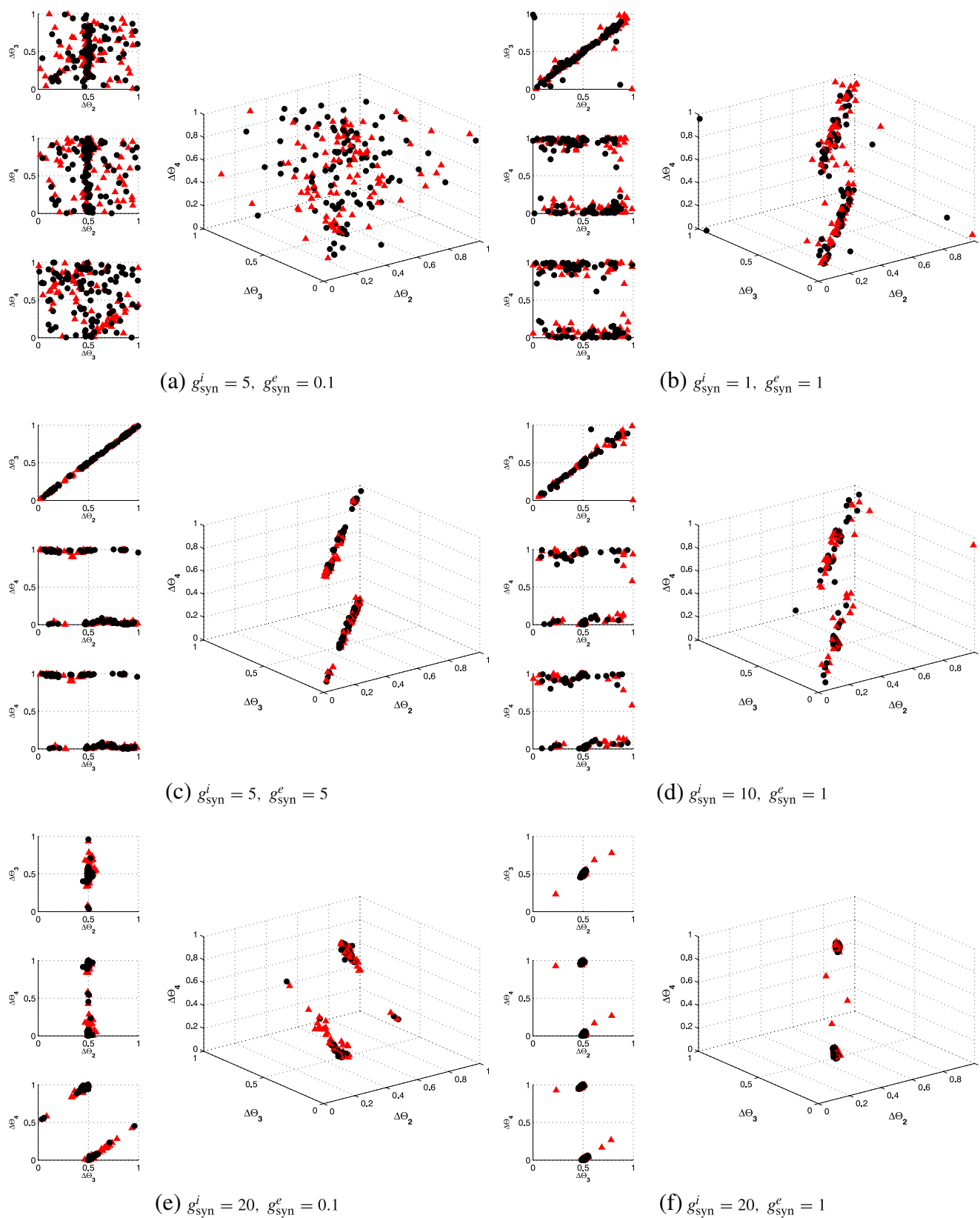distance to hopping rises fairly quickly to its plateau
value.

(a) $g_{syn}^i = 5$, $g_{syn}^e = 0.1$

(b) $g_{syn}^i = 1$, $g_{syn}^e = 1$

(c) $g_{syn}^i = 5$, $g_{syn}^e = 5$

(d) $g_{syn}^i = 10$, $g_{syn}^e = 1$

(e) $g_{syn}^i = 20$, $g_{syn}^e = 0.1$

(f) $g_{syn}^i = 20$, $g_{syn}^e = 1$

Fig. 11 Relative phasing of bursts in the 4-CE model for various coupling strengths, starting from 100 random initial phase configurations. *Red triangles* indicate phasing after three burst cycles; *black circles* indicate phasing after eight burst cycles. Results for the 4-IRCE model at the same combinations of g_{syn}^i and g_{syn}^e are nearly identical
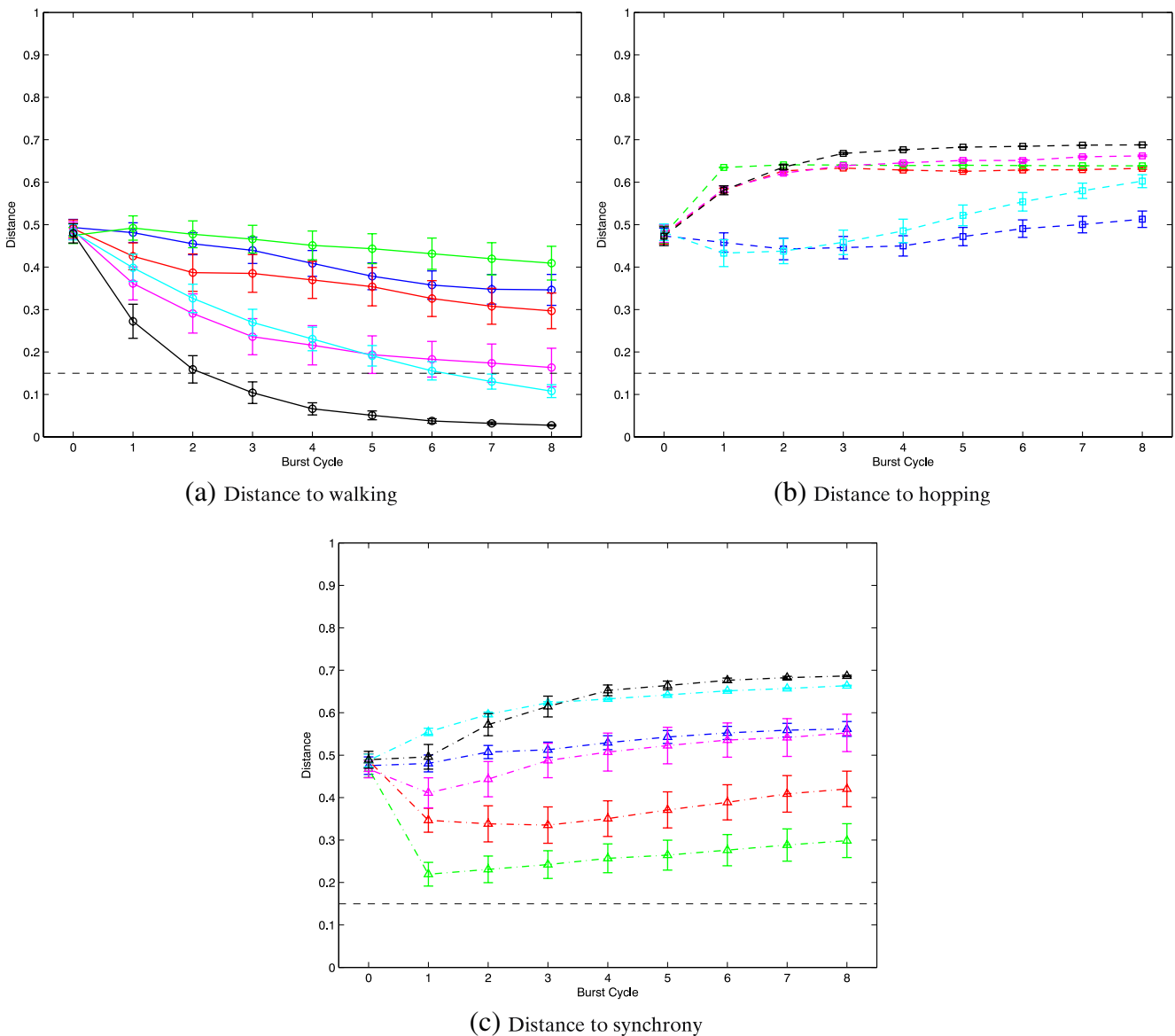
(a) Distance to walking

(b) Distance to hopping

(c) Distance to synchrony

Fig. 12 Mean distance to target phasing configurations—(**a**) walking, (**b**) hopping, (**c**) synchrony—after each burst cycle in simulations of the 4-CE model for various various coupling strengths. The *horizontal dashed black line* indicates the threshold for convergence to the target configuration. *Error bars* in-dicate variance; line color indicates coupling strength. (1) *Blue*: $g_{syn}^i = 5$, $g_{syn}^e = 0.1$. (2) *Red*: $g_{syn}^i = 1$, $g_{syn}^e = 1$. (3) *Green*: $g_{syn}^i = 5$, $g_{syn}^e = 5$. (4) *Magenta*: $g_{syn}^i = 10$, $g_{syn}^e = 1$. (5) *Cyan*: $g_{syn}^i = 20$, $g_{syn}^e = 0.1$ (6) *Black*: $g_{syn}^i = 20$, $g_{syn}^e = 1$

The lack of clustering along the $\Delta\theta_2 + \Delta\theta_3 \approx 0$ mod 1 line indicates that the synchronization due to ex-citation does not help the ipsilateral neuron pairs anti-synchronize. That is, the effects of excitation and (sym-metric) inhibition are more or less independent of one another at lower coupling strengths; strong excitatory coupling in combination with moderately strong sym-metric inhibition, may be counterproductive, however. For $g_{syn}^i = 5$, $g_{syn}^e = 5$, Fig. 11(c), after rapid alignment on the contralateral flexor-extensor synchrony axis, the relative phases move quite slowly. As can be seen from

Fig. 12(a), for this set of coupling strengths the models' mean distance to walking decreased monotonically, but very slowly; in terms of convergence rate to walking this inhibition/excitation combination performs worst.

Looser alignment along the contralateral flexor-extensor synchrony axis is seen in the same regime of moderately strong inhibition and excitation when inhibition is stronger than excitation (Fig. 11(d)). The models' behavior in this case is similar to that for inter-mediate inhibition and excitation (cf. Fig. 11(b), and the red (2) and magenta (4) lines in Fig. 12), but with more

rapid convergence towards walking. After aligning on the $\Delta\theta_4 \approx 0 \mod 1$, $\Delta\theta_2 \approx \Delta\theta_3 \mod 1$ axis, the phases begin to achieve the walking configuration after about 8 cycles.

With stronger inhibition but weak excitation (e.g. $g^i_{\text{syn}} = 20$, $g^e_{\text{syn}} = 0.1$, Fig. 11(e)), the models' relative phases do not move as rapidly towards contralateral flexor-extensor synchrony. Instead, the relatively stronger inhibition first draws the phases towards the line of ipsilateral flexor-extensor alternation, $\Delta\theta_2 \approx 0.5$, $\Delta\theta_3 - \Delta\theta_4 \approx 0.5 \mod 1$, and in a fashion similar to the asymmetric 4-IR model with stronger ipsilateral inhibition (cf. Fig. 9(b)), the 4-CE and symmetric 4-IRCE models begin to converge towards the walking configuration along this line, doing so more rapidly for stronger excitation. (The effect of the additional inhibitory synapses in the symmetric 4-IRCE model is small, but noticeable for these combinations of coupling strengths: they produce slightly faster convergence to the walking configuration.) From a very small number ($\approx 3\%$) of initial conditions, the model converges to the hopping configuration after eight burst cycles.

The 4-CE and symmetric 4-IRCE models reach the walking configuration fairly rapidly from every initial condition for $g^i_{\text{syn}} = 20$, $g^e_{\text{syn}} = 1$ (Fig. 11(f)). Within 3 cycles, the models' mean distance to walking falls below 0.15, and within 5 cycles, both models' phases cluster tightly within a radius of 0.06 about $\Delta\theta_2 = \Delta\theta_3 = 0.5$, $\Delta\theta_4 = 0$. (Note that relative phasing is shown in Fig. 11(f) only after the third and eighth burst cycles.) When excitation is increased, however, the convergence slows considerably (not shown). The phases first align along the contralateral flexor-extensor synchrony axis, then move towards the walking configuration, which is reached only after 7–8 cycles, rather than 3–5, a result similar to that shown in Fig. 11(d).

The differences in convergence seen in the 4-CE and symmetric 4-IRCE models at various combinations of strong coupling can be understood in terms of the relative 'phasing speeds' of inhibition and excitation and competition between the two types of coupling. Inhibition acts more slowly than excitation: even at the highest levels of inhibition, the antiphase configuration is reached only after 2–3 cycles, whereas strong excitation can cause neurons to synchronize within 1–2 cycles. Once excitation has synchronized two neurons, inhibition must move both of them towards antiphase (relative to a third neuron) simultaneously. The synchronized pair may effectively act like a single, 'heavier' neuron that is more intransigent and less responsive to the 'pushes' that inhibition imparts to it than individual, unsynchronized neurons would be at the same coupling strengths. If, for example, the contralateral flexor-

extensor pairs are synchronized but the ipsilateral flexor-extensor pairs are not anti-synchronized, then inhibition on either side may actually work against inhibition on the other, depending on the relative phasing of the contralateral pairs. Conversely, if the ipsilateral neurons are already set in the antiphase configuration by inhibition, this impedes the contralateral synchronization activity of excitation, which may have to disrupt the antiphase configurations on each side in order to synchronize flexors and extensor on opposite sides. Just as excitation opposes inhibition's disruption of synchrony in the other situation, inhibition opposes the disruption of antisynchrony by excitation in this case. Thus too much excitation relative to inhibition, and vice versa, may slow the models' approach to the walking configuration. There is an optimal balance of symmetric inhibition and excitation around $g^i_{\text{syn}} = 20$, $g^e_{\text{syn}} = 1$.

Asymmetric inhibition For low levels of excitation, i.e. $g^e_{\text{syn}} \leq 0.01$, asymmetric inhibition in the 4-IRCE model produces phasing behavior very similar that of the asymmetric 4-IR model at the same levels of ipsilateral and contralateral inhibition (cf. Fig. 9). Intermediate to strong excitation ($g^e_{\text{syn}} \geq 0.1$) acts to accelerate the convergence of the model to the walking mode. Combinations of $g^{i,i}_{\text{syn}}$ and $g^{i,c}_{\text{syn}}$ that produce alignment of relative phases in the asymmetric 4-IR model along either $\Delta\theta_3 \approx 0.5 \mod 1$, $\Delta\theta_2 - \Delta\theta_4 \approx 0.5 \mod 1$ (rhythmic left-right alternation to walking) or $\Delta\theta_2 \approx 0.5 \mod 1$, $\Delta\theta_3 - \Delta\theta_4 \approx 0.5 \mod 1$ (hopping to walking) produce similar alignment in the asymmetric 4-IRCE model (Fig. 13(a) and (b)). With the additional excitation, the asymmetric 4-IRCE then model converges along these axes to the walking mode within about 8 burst cycles, doing so slightly more rapidly when contralateral inhibition is stronger than ipsilateral inhibition (Fig. 14).

Intermediate excitation ($g^e_{\text{syn}} \geq 1$) in combination with the appropriate balance of (asymmetric) ipsilateral and contralateral inhibition ($g^{i,i}_{\text{syn}} \geq 10$, $g^{i,c}_{\text{syn}} \geq 5$) produces rapid convergence (within 2–3 burst cycles) to walking, as seen in Fig. 13(c). This is half the amount of inhibition needed to produce comparable convergence to walking in the symmetric 4-IRCE model at the same level of excitation. Rapid convergence occurs for asymmetric inhibition in this range regardless of whether contralateral or ipsilateral inhibition is stronger, though the model converges fastest with strong excitation and stronger contralateral than ipsilateral inhibition, as seen in Figs. 13(d) and 14(a). Rather than accelerating convergence to the walking mode, increasing excitation beyond $g^e_{\text{syn}} = 1$ in the asymmetric 4-IRCE model may somewhat impair convergence, as

(a) $g_{syn}^{i,i} = 5$, $g_{syn}^{i,c} = 15$, $g_{syn}^e = 0.1$

(b) $g_{syn}^{i,i} = 20$, $g_{syn}^{i,c} = 5$, $g_{syn}^e = 0.1$

(c) $g_{syn}^{i,i} = 20$, $g_{syn}^{i,c} = 5$, $g_{syn}^e = 1$

(d) $g_{syn}^{i,i} = 20$, $g_{syn}^{i,c} = 40$, $g_{syn}^e = 1$

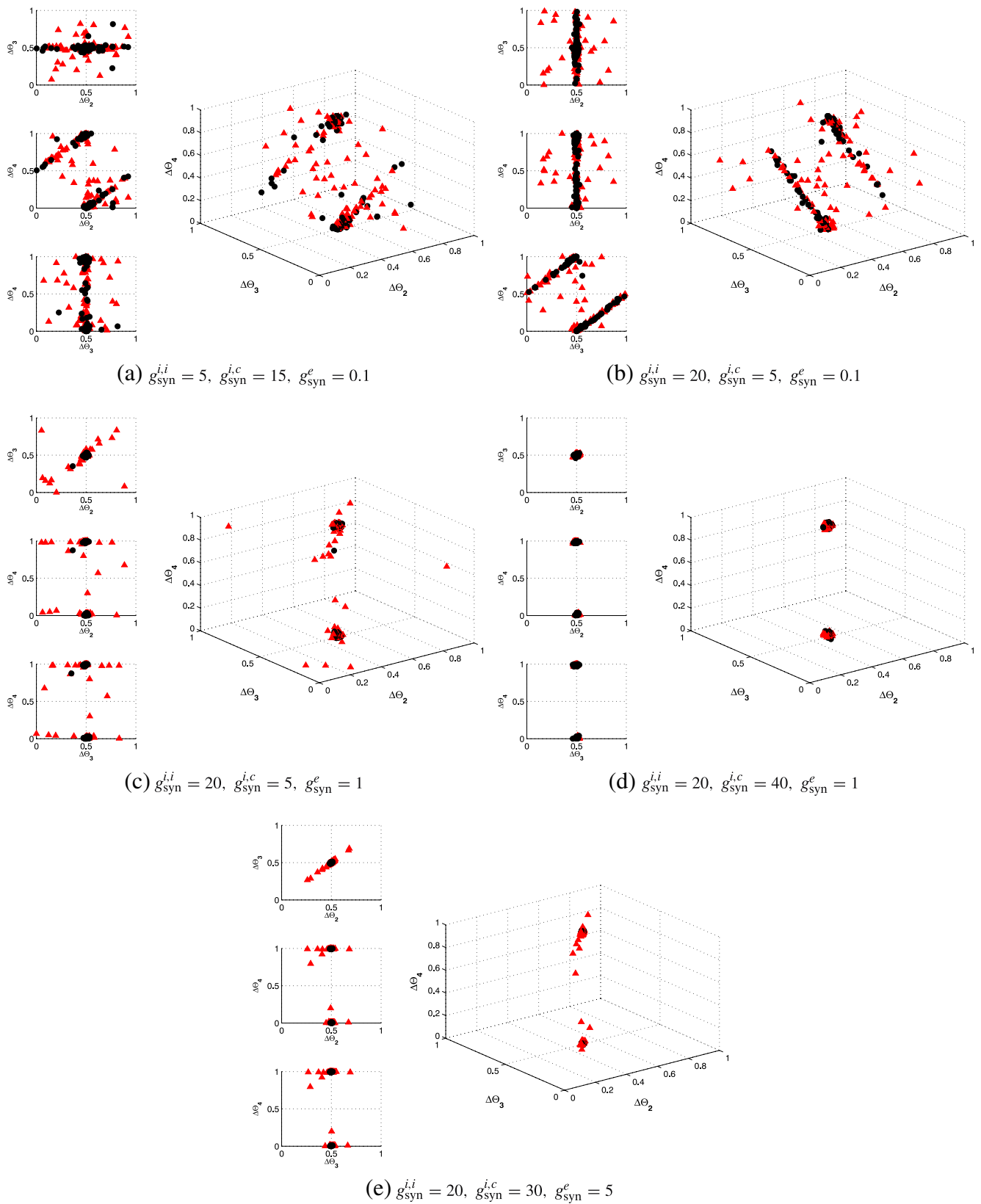(e) $g_{syn}^{i,i} = 20$, $g_{syn}^{i,c} = 30$, $g_{syn}^e = 5$

Fig. 13 Relative phasing of bursts in the 4-IRCE model with separately varying levels of ipsilateral and contralateral inhibition, starting from 100 random initial phase configurations. *Red triangles* indicate phasing after three burst cycles; *black circles* indicate phasing after eight burst cycles
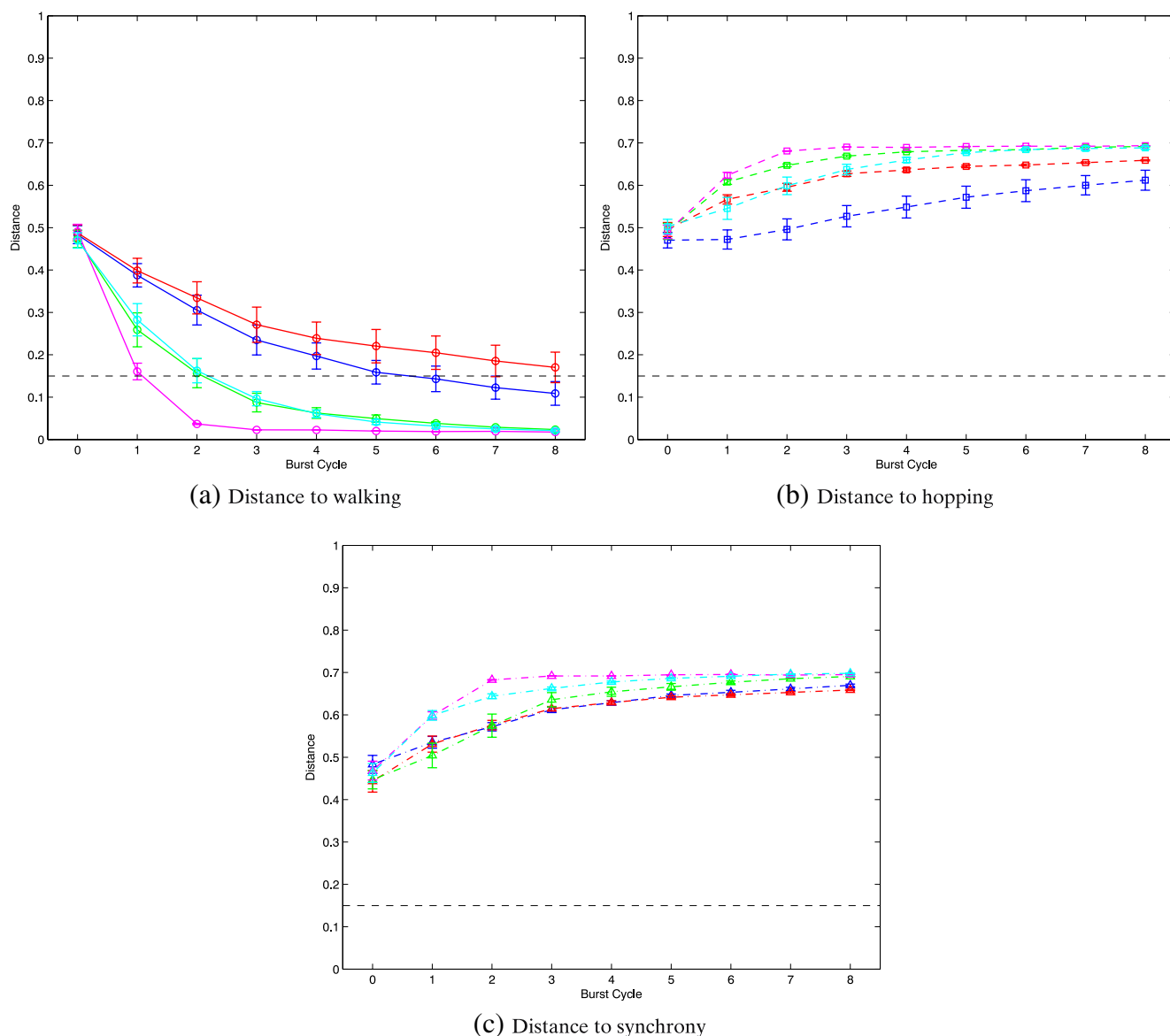
(a) Distance to walking

(b) Distance to hopping

(c) Distance to synchrony

Fig. 14 Mean distance to target phasing configurations—(**a**) walking, (**b**) hopping, (**c**) synchrony—after each burst cycle in simulations of the 4-IRCE model for various various coupling strengths. The *horizontal dashed black line* indicates the threshold for convergence to the target configuration. *Error bars* indicate variance; line color indicates coupling strength.

(1) *Blue*: $g_{syn}^{i,i} = 5$, $g_{syn}^{i,c} = 15$, $g_{syn}^{e} = 0.1$. (2) *Red*: $g_{syn}^{i,i} = 20$, $g_{syn}^{i,c} = 5$, $g_{syn}^{e} = 0.1$. (3) *Green*: $g_{syn}^{i,i} = 20$, $g_{syn}^{i,c} = 5$, $g_{syn}^{e} = 1$. (4) *Magenta*: $g_{syn}^{i,i} = 20$, $g_{syn}^{i,c} = 40$, $g_{syn}^{e} = 1$. (5) *Cyan*: $g_{syn}^{i,i} = 20$, $g_{syn}^{i,c} = 30$, $g_{syn}^{e} = 5$.

it also does in the case of symmetric inhibition. The greater excitation induces the neurons' relative phases to align along $\Delta\theta_4 \approx 0 \mod 1$, $\Delta\theta_2 \approx \Delta\theta_3 \mod 1$ immediately, as seen in Fig. 13(e), then inhibition moves the relative phases along this axis towards the walking configuration within three burst cycles, producing final convergence behavior very similar to that for stronger ipsilateral than contralateral inhibition and lower excitation, $g_{syn}^{i,i} = 20$, $g_{syn}^{i,c} = 5$, $g_{syn}^{e} = 1$. These results support the idea that the synchronizing effect of excitation

is stronger and more rapid than the antisynchronizing action of inhibition at comparable synaptic strengths.

3.4 Summary

The full CPG model is capable of reproducing the fundamental locomotor rhythm, but convergence to walking is rather slow and the model's performance depends sensitively on the balance of connection strengths among several critical synapses, and on its initial

phasing configuration. Strong reciprocal inhibition between ipsilateral flexor and extensor RGNs is necessary for convergence in biologically reasonable time, as is strong cross-cord inhibition between certain CIN-CIN and CIN-RGN pairs. Weak to moderate cross-cord excitation has a substantial modulatory effect on the full model's convergence behavior. For the various key synapses, higher strengths generally correlate positively with more rapid convergence to the fundamental locomotor rhythm.

Strong inhibition is needed in order for two reciprocally coupled RGNs to achieve antisynchrony in eight or fewer burst cycles; somewhat weaker reciprocal excitation is needed to achieve synchrony in the same time frame. For both reciprocal inhibition and excitation, higher coupling strengths produce more rapid convergence to the final configuration, but convergence is non-monotonic: the relative phasing of the coupled neurons may shift in a seemingly erratic fashion for some time before the neurons achieve stable (anti)synchrony.

Four-cell networks require strong ipsilateral and contralateral inhibition in order for coherent locomotor patterns to emerge. In general, higher synaptic strengths lead to faster convergence. In the absence of excitation, symmetric ipsilateral and cross-cord inhibition favors convergence to the hopping configuration; substantially stronger contralateral than ipsilateral inhibition produces walking. Reciprocal cross-cord flexor-extensor excitation significantly accelerates convergence to walking in four-cell networks with symmetric ipsilateral and contralateral inhibitory connections, as well as in those with asymmetric inhibitory configurations. Convergence to the fundamental locomotor rhythm occurs most rapidly in networks combining strong reciprocal ipsilateral flexor-extensor inhibition, stronger contralateral flexor-flexor/extensor-extensor inhibition, and moderate reciprocal cross-cord flexor-extensor excitation. Among the models we tested, the asymmetrical 4-IRCE model performs best as measured by convergence speed and stability of the walking mode.

4 Discussion

We have developed a model of the RSHL CPG as a network of coupled oscillators, incorporating empirical data to construct the network from conductance-based model neurons that are synaptically coupled according to functional connection patterns inspired by anatomical and electrophysiological studies. We investigated the model's ability to generate the basic walking gait,

and its convergence and phase resetting behavior. Our model stably reproduces the fundamental locomotor walking rhythm, viz. ipsilateral alternation between flexor and extensor bursts simultaneous with contralateral synchronization of flexor and extensor bursts, but it does not meet our expectations for robustness or rapid recovery to this rhythm after perturbation. In dynamical terms, the domain of attraction for the fundamental locomotor rhythm is small and convergence of nearby trajectories to this rhythm requires the equivalent of many steps. These results provide insight into the organization of the RSHL CPG.

The specific location, structure and organization of spinal CPGs remain unknown. Model simulations are one way to test ideas about this organization and to develop hypotheses for further scrutiny. The models studied in this paper are based on networks in which four independent oscillators each drive extensor and flexor muscle groups on right and left hindlimbs. These oscillators are coupled to one another synaptically through interneurons in our twelve cell model and directly in our four-cell models. These architectures resemble abstract networks of coupled oscillators in which the coupling coordinates the phases among the oscillators but plays little role in determining the amplitude or stability of the limit cycles produced by each oscillator. Mathematical analysis of these models is customarily reduced to interactions of the phases. Our models bring more biological structure to these classes of models. For simplicity, we chose each oscillator to be a bursting neuron that fires action potentials during its active phase and coupled these neurons with "standard" model synapses. We found that the effective phase coupling in these models is weak, suggesting that either some of our hypotheses about fictive locomotion are wrong or that the particular model architectures that we studied are poor representations of the organization of the RSHL CPG.

It is frequently said that models are more useful when they are wrong than when they are right. Below we review some of our modeling ansätze, namely the use of endogenously bursting model neurons as component oscillators and the coupling of these oscillators according to highly symmetric network architectures, in light of our models' performance. Our findings prompt questions about why the models behave in the manner we observed and suggest experiments which could test organizational properties of the RSHL CPG that distinguish models of the type studied in this paper from alternatives.

Model oscillators In the unit burst generator rubric under which our models fall, the CPG for hindlimb

movement is distributed along the spinal cord in a modular fashion, with UBGs capable of independent oscillation controlling individual joints or synergistic muscle groups. The original formulation of the UBG hypothesis is agnostic with regard to the rhythmogenic mechanism underlying each UBG's bursting behavior, and positing that "it is likely that CPGs operate with several, possibly redundant mechanisms assuring an appropriate pattern generation under a variety of conditions" (Grillner 1981). We model each flexor and extensor UBG as a single endogenously bursting neuron (RGN) with one slow variable, so that the active segment of each RGN's endogenous burst represents the total activity of its respective UBG module (which in turn represents a group of neurons whose combined oscillatory activity could arise through any number of mechanisms). The interaction of flexor/extensor UBG modules to produce the CPG's output is thus reduced to the interaction of single bursters.

An alternative configuration is the classic half-center oscillator, wherein two tonically spiking neurons are coupled via reciprocal inhibition, with one neuron representing a flexor oscillator and the other an extensor oscillator. The two cells alternate between flexor (respectively, extensor) activity and extensor (respectively, flexor) silence as the inactive cell either escapes or is released from suppression by the currently active cell. Standard phase-plane analyses of frequency and phasing control in half-center networks rely on a reduction to a coupled relaxation oscillator regime in which the relative positions of the oscillators' fast and slow nullclines determine the cells' activity patterns (Skinner et al. 1994; Rowat and Selverston 1997). Daun et al. use this technique in a recent paper to compare the range of oscillation periods in half-center oscillators built of component neurons having a variety of intrinsic oscillatory (spiking) mechanisms, including an I_{NaP}-based mechanism related to our RGN model (Daun et al. 2009). These studies have elucidated the roles of escape and release in half-center networks' responses to excitatory inputs, such as tonic drive, and in control of network oscillation frequency. In particular, the intrinsic mechanisms underlying their component neurons' oscillations may play a significant role in determining the networks' range of oscillation frequencies and response to asymmetric drives. These functional characteristics may constrain the intrinsic properties of component neurons in half-center oscillator CPG models.

Though the classic half-center oscillator and the 2-I network, for example, are diagrammatically similar, results from analyses of half-center oscillator models cannot be directly applied to the coupled UBG models we study in this paper. Geometrically and dynamically speaking, spiking and bursting neuronal models—coupled or uncoupled—are qualitatively dissimilar, and this dissimilarity is a consequence of the separation of time scales effected by a slowly evolving dynamic variable, rather than the presence of any specific current (Rinzel and Lee 1987; Rinzel 1987; Izhikevich 2000). The dynamics of bursting and relaxation oscillations are not equivalent, the behavior of coupled bursters may be quite complex, and half-center oscillator phase-plane analyses do not naively carry over to the case of coupled bursters (Best et al. 2005; De Vries and Sherman 2005; Sherwood 2008; Sherwood and Guckenheimer 2009). (The four and twelve-cell models we consider also combine inhibitory and excitatory coupling, further confounding the sort of analysis performed for half-center oscillatory networks.)

The salient factor for our RSHL CPG models consists of the phase response properties of the bursting neurons comprising the models' oscillators. We have studied these properties and report our findings in detail elsewhere (Sherwood 2008; Sherwood and Guckenheimer 2009). These mathematical studies are based upon the concept of *isochrons*, sets of points approaching a limit cycle with the same asymptotic phase. Phase response curves describe the change in asymptotic phase produced by an input that moves the state of the system off the limit cycle and are determined by the geometry of the system's isochrons. Here the inputs are the post-synaptic response to an action potential in a pre-synaptic cell.

The phase response of our model neurons is highly sensitive to the amplitude and phase of the input. As a general rule of thumb, we find that the largest phase responses come from those that alter the number of spikes during the active phase of a bursting oscillation. Large synaptic inputs are required to produce changes in the active burst length. Excitatory inputs have a larger effect than inhibitory inputs, particularly near the initiation of the active phase of a burst. These phase response characteristics are found in a wide range of bursting neural models, and are related to the high degree of curvature for isochrons of bursting—but not tonically spiking—neural models (Sherwood 2008; Sherwood and Guckenheimer 2009). The influence of phase response sensitivity permeates the results that we found in all of the two, four, and twelve-cell networks that we studied. Our findings prompt further investigation of the phase response curves of bursting neurons. Do real oscillatory neurons have the extremely sensitive phase responses of the model neurons studied here? What factors in model neurons contribute to sensitive phase responses? Does physical separation

of synapses from the conductances underlying spiking ameliorate the sensitivity of phase responses? Answers to these questions will help resolve whether UBGs comprising endogenously bursting neurons alone can be adequate building blocks for realistic locomotor CPG models; the results presented in this paper hint that this may not be so.

Network architectures   In accordance with the theory of coupled cell networks, all of the CPG architectures examined were highly symmetric; those networks with unequal ipsilateral and contralateral flexor-extensor coupling strengths retained their bilateral symmetry. The extent to which the biological CPG possesses such symmetries is unknown, and evidence from normal locomotor function indicates more limited cross-cord coupling symmetry: as seen in both intact and de-cerebrate animals receiving midbrain stimulation, the stance phases of the left and right legs overlap during walking, and ipsilateral flexors and extensors may maintain different periods, enabling smooth variation of walking speed without changing gait (Pearson and Rossignol 1991; Yakovenko et al. 2005; Endo and Kiehn 2008). The asymmetric activation of flexors and extensors suggests that for animals capable of normal gaits, the functional strength of inhibitory and/or excitatory coupling between left and right flexors may be rather different than that between left and right extensors. Thus, though it is their symmetry properties that connect our models to mathematical theory, our models' symmetries may be viewed as artificially limiting the models' ability to reproduce the full range of realistic locomotor patterns found in intact animals. The experiments which primarily inform our modeling efforts—fictive locomotor experiments in which the whole spinal cord is removed, and thus all sensory input is lost—concern a much more limited range of locomotor-like behavior, however, and recordings from ventral root motoneuron bundles at the L2 and L5 segments during these experiments display more substantial symmetry between periods of flexor and extensor activation than what is seen in experiments in which the CPG is not isolated from sensory feedback (Kiehn and Kjaerulff 1996, 1998; Kiehn et al. 2000; Kiehn and Butt 2003). Bearing in mind that the biological network may not share all the symmetries of the models, we consider implications of our modeling results for the organization of synaptic coupling in the RSHL CPG.

It is clear from laboratory experiments that inhibition plays an important role in patterning the activity of the rodent lumbar spinal cord. Inhibition alone could suffice to generate the walking rhythm in our models. However, the four-cell network without excitation,

4-IR, rapidly converged to the fundamental locomotor rhythm only when overall inhibition levels were extremely high and contralateral inhibition was 50% greater than ipsilateral inhibition. When ipsilateral inhibition was equal to or greater than contralateral inhibition (and overall inhibition was very strong), the 4-IR preferentially converged to the hopping configuration. (We note that the strong preference for hopping cannot be deduced by solely considering the symmetries of the network: the square symmetry of the symmetric 4-IR model makes analysis of the set of admissible oscillatory configurations particularly involved (Swift 1988), and were the dynamics of the RGN oscillators reducible to those of simple phase oscillators, a stable hopping configuration would not be predicted (Golubitsky et al. 2006).) Other four-cell models required high ratios of inhibition to excitation to converge to the fundamental locomotor rhythm in biologically reasonable time. In particular, strong reciprocal inhibition between RGNs was necessary to obtain ipsilateral flexor-extensor alternation. Moderate cross-cord excitation also significantly accelerated convergence of the 4-CE and 4-IRCE models to the fundamental locomotor rhythm, as compared to the behavior of the 4-IR model at identical levels of inhibition. These results point to a requirement for strong inhibition vis-à-vis excitation to set the proper phasing of rhythmically oscillatory neurons in the CPG.

Symmetric coupling, specifically equally strong contralateral and ipsilateral inhibition, appeared to degrade the four-cell models' convergence to the fundamental locomotor rhythm. In the symmetric 4-IR model, the default phase configuration was hopping, rather than walking, and for a given level of excitation, the asymmetric 4-IRCE model converged to the walking mode faster than the symmetric 4-IRCE model. Comparison of the output from the 4-CE and symmetric 4-IRCE models indicated that cross-cord intrasegmental reciprocal inhibition played no noticeable role in establishing flexor-flexor/extensor-extensor alternation. Instead, comparatively low levels of excitation rapidly synchronized contralateral flexor-extensor pairs. The biological network does not react in this way: Whole-cord experiments in which fictive locomotor activity is first induced by bath application of neuromodulators (5-HT, NMDA, DA), and then inhibitory synaptic inputs are pharmacologically blocked typically result in synchronous intrasegmental left-right activity. The better performance of the asymmetric models and the inconsistency of their symmetric counterparts' behavior with laboratory experiments lead us to suspect that abstract CPG models which rely on network symmetries for analysis may have limited success in capturing the

behavior of specific biological CPGs (cf. Buono and Golubitsky 2001; Buono 2001).

Taken together, the findings above suggest that intrasegmental cross-cord inhibition may be functionally much stronger than ipsilateral intersegmental inhibition. In this scenario, the primary function of ipsilateral intersegmental inhibition is to establish the initial alternation of flexors and extensors on each side. Once they burst rhythmically in antiphase, ipsilateral interneuron pools driving flexors and extensors could maintain their phasing without significant drift in the absence of additional inhibition or confounding excitatory inputs. The participation of independent subpopulations of endogenous bursters in each segment might contribute to ipsilateral flexor-extensor phase stability. Our models predict that ipsilateral intersegmental inhibition would still need to be quite strong to effect the initial flexor-extensor alternation; the strength of cross-cord connections would determine whether hopping or walking is the system's preferred locomotive mode. If cross-cord inhibition is the predominant means for effecting left-right alternation, then the 4-IR model suggests that it must be significantly stronger than ipsilateral inhibition in order for walking, rather than hopping, to be the default configuration. Or cross-cord excitatory connections that promote synchrony between contralateral flexor- and extensor-phased interneuron groups could play the primary role in disposing the system to walk, as in the 4-CE and 4-IRCE models. In this case, cross-cord inhibition could be relatively weak, but we would not predict blocking inhibition to lead to cross-cord synchrony unless there was also (possibly weak) intrasegmental cross-cord excitation, which has been observed anatomically and from electrophysiological experiments (Quinlan and Kiehn 2007). Transgenic mouse lines in which particular groups of excitatory or inhibitory interneurons are rewired or are missing (Kiehn and Kullander 2004; Lanuza et al. 2004; Goulding and Pfaff 2005; Kiehn 2006) are promising tools for investigating these various possibilities. As an example, increasing crossed excitation in EphA4 mutant mice enhances intrasegmental left-right synchrony, resulting in a hopping gait, and pharmacologically increasing crossed inhibition in the mutant mice can restore the normal left-right alternation (Dottori et al. 1998; Kullander et al. 2003). Our simulations are consistent with these results if the miswiring due to loss of EphA4 results in increased intrasegmental (flexor-flexor and extensor-extensor) excitatory coupling (Yokoyama et al. 2001; Butt et al. 2005).

How does the biological CPG switch quickly from one gait to another? Neuromodulation may rapidly alter the balance between two or more synaptic subsets which each tend to push the system towards a different locomotor configuration. There are manifold possibilities for shifting from one particular gait to another. For instance, if the default CPG walking program were maintained by a combination of asymmetric inhibition and cross-cord excitation similar to that of the 4-IRCE model, then a switch from walking to hopping could be effected by selectively weakening cross-cord flexor-extensor excitation and strengthening ipsilateral flexor-extensor inhibition to bring the CPG to a configuration resembling the symmetric 4-IR model, which preferentially hops. If walking were normally produced by a purely inhibitory network like the asymmetric 4-IR model, then similar neuromodulatory rebalancing towards inhibitory symmetry should have the same effect. Alternatively, sufficiently strong activation of cross-cord (intrasegmental flexor-flexor/extensor-extensor) excitatory connections may reset the CPG's gait to hopping. The models we studied responded more rapidly to changes in excitation than to changes in inhibition; we suggest that gait selection in the real CPG may be accomplished primarily through neuromodulation of various subsets of excitatory synapses, rather than by changing the strength of inhibition. Evaluating the biological plausibility of this hypothesis requires a more comprehensive and detailed profile of CPG anatomy and physiology than is currently available.

Alternative modeling approaches The CPG models studied in this paper are more biophysically realistic elaborations than abstract, analytically tractable coupled oscillator models that were expected to produce the fundamental locomotor rhythm largely due to symmetry properties. Our 'minimalist' approach increases model complexity incrementally to aid in elucidating which model features are necessary in order to reproduce a limited set of behaviors experimentally observed in the biological CPG. Further along the continuum of complexity are large scale models that incorporate large amounts of experimental data and which attempt to reproduce a broad range of locomotor patterns observed under a wide range of conditions.

In this vein, Rybak et al. have recently developed a model of the mammalian spinal locomotor CPG (Rybak et al. 2006a, b) based on experiments involving stimulation of afferent sensory pathways and spontaneous 'deletions' in which some motoneuron pools fail to fire for one or more cycles, then resume their normal activity (Lafreniere-Roula and McCrea 2005; McCrea and Rybak 2007). This model stably reproduces the pattern of motoneuron burst phasing seen in fictive locomotor preparations from decerebrate cats, including responses to afferent sensory stimulation and

spontaneous deletions, and it reproduces the biological range of locomotor cycle frequencies and flexor-extensor phase durations as the strength of higher level excitatory drive is varied.

In contrast to our CPG models, the model of Rybak et al. possesses rapid phase resetting properties and does not exhibit sensitive phase responses. Their model is substantially more complex than ours, and the two models have several significant differences: (1) Their underlying neuron models are more complicated, possessing more intrinsic currents and multiple compartments (though I_{NaP} was also the key slow current in their model rhythmogenic neurons). (2) Rhythmogenesis, pattern formation, and motor output are performed in separate network layers, such that the rhythmogenic layer receives tonic drive with no feedback from the pattern-generating layer, and oscillatory activity of rhythmogenic layer half-centers is modified by the pattern generation layer prior to the motoneuronal level. (3) Motoneuronal output feeds back to the motoneurons and to higher levels via inhibitory interneurons. (4) Motoneuron and interneuron pools are modeled by populations having distributions of intrinsic properties, rather than single neurons. (5) Synapses are modeled with alpha functions instead of an autonomous synapse model with presynaptic voltage-dependent neurotransmitter release.

The contrast between the structure and output of their full-featured, complex model and those of our minimal model offers an opportunity to explore which architectural features and intrinsic mechanisms are responsible for particular phasing and gait control properties in the mammalian spinal locomotor CPG. It is possible to vary the period and duty cycle of the RGN oscillators in our models by changing tonic drive or by modulating I_{NaP} or the leak current, thus changing in the speed of the locomotor cycle. Changing synaptic weights alone does not substantially change locomotor cycle frequency. We do not expect changing the locomotor cycle speed via modulation or external drive to ameliorate the models' slow convergence to walking nor to alter the models' phase resetting properties substantially; our investigations along these lines support this view. Recent experiments indicate that a specific class of ventral interneurons, V2a, is responsible for ensuring proper left-right alternation during high speed locomotion (Crone et al. 2008, 2009), acting to increase functional inhibition between left and right hemicords at higher speeds. One hypothesis is that the functional strength of the commissural excitatory pathway increases with locomotor speed, and the V2a interneurons act to maintain the proper balance between cross-cord inhibition and excitation. Our models

required strong contralateral inhibition to produce a walking gait at a single fixed speed. An avenue for exploration, which could be pursued comparatively with our models and the model of Rybak et al., would be to investigate convergence and gait-switching behavior as both oscillator frequency and synaptic strength are dynamically modified.

It seems likely that both the separation of rhythmogenesis from pattern formation and the mixing of traditional half-center and unit burst generator architectures contribute to the robust phasing attributes of the Rybak et al. model, including rapid recovery from deletions. Analyses of more abstract models of gait production indicate that UBG-based architectures should suffice to stably reproduce and switch among a variety of basic locomotor rhythms, without requiring multiple network layers, but our single-layer models' slow performance at these tasks prompts us to ask whether (or how) the multilayer structure of the Rybak et al. model promotes rapid convergence to walking gaits and rapid resetting in response to perturbations. Other aspects of the Rybak et al. model may contribute to these features.

The experimental evidence for deletions, in particular the observation that the spinal cord returns to its original phase after a few perturbed cycles, supports the hypothesis that the biological CPG has a multi-level structure such as the one instantiated in the Rybak et al. model, where a higher level rhythmogenic 'clock' drives a pattern formation layer with periodic excitatory input. In contrast, there is no obvious means for robustly generating spontaneous locomotor rhythm deletions in either the four-cell or twelve-cell networks studied here. Though deletions are not among the output patterns our single-layer models were intended to reproduce, such behavior could conceivably be obtained using the same synaptic architecture in conjunction with oscillators having more complex intrinsic dynamics. Neither current mathematical theory nor experimental data provide precise guidance for altering the neurons' intrinsic properties to achieve this aim, however. It is possible that strong, periodic excitatory inputs could act to organize the phase relationships among the RGNs in our models. One modeling suggestion would be to treat our current models as a pattern formation layer and provide appropriately timed periodic inputs to the RGNs. Improved convergence behavior from such a configuration would further support the idea of a multilayer CPG.

Our models suggest that a CPG architecture composed purely of UBGs requires functionally strong synaptic inputs to effect rapid phase resetting. The difference in synapse models precludes direct compar-

ison of synaptic strengths between CPG models; it is unclear whether the synaptic coupling in the Rybak et al. model is effectively weak or strong according to our classification scheme. We have investigated the effect of synapse model type on phase response and have found that the fine details of phase response may vary significantly with synapse model (Sherwood 2008), but this subject deserves further study. Post-synaptic currents have been measured in some spinal motoneurons and interneurons under various conditions (Raastad et al. 1997; Zhong et al. 2007), but there has been no systematic survey of the strength of coupling between identified subpopulations of spinal neurons. A complete map of the spinal synaptic architecture is far too much to ask for, but additional experimental data regarding the strength of cross-cord commissural inhibition and excitation could help substantially to distinguish between model alternatives and to improve model revisions.

The weak phase stability of our models has not been directly tested in fictive locomotion. It is known that sensory feedback has the capacity to immediately reset the locomotor rhythm for walking (Hultborn et al. 1998), and that feedback connections in the propriospinal network modify the basic CPG rhythm during normal locomotion (Sqalli-Houssaini et al. 1993), but perturbation experiments have not been performed with the isolated spinal cord preparations that we model. Nonetheless, we expect that we would obtain similar results if our models were modified to include feedback from MNs to RGNs. Very large inputs are required to initiate or terminate bursts abruptly in our model RGNs. The slow variable underlying the oscillations in these cells is the gating variable for persistent sodium current, and this is not affected directly by synaptic inputs. If the spinal CPG does consist of independent endogenous oscillators, then our observations suggest that bursting is supported by a richer set of intrinsic conductances that allow these cells to be switched from active to inactive states rapidly by a synaptic input. An alternative hypothesis, is that the spinal CPG does not consist of independent oscillators. One possibility is that flexor-extensor alternation is produced by reciprocal inhibition of (subnetworks of) neurons that fire tonically in isolation (as in the Rybak et al. model), or that burst by mutual excitation and fatigue.

Yet another alternative hypothesis is that the phase resetting properties of the RSHL CPG depend upon network properties, specifically that they depend upon networks of coupled heterogeneous oscillatory neurons, or neurons with varying post-inhibitory rebound. Further work is needed to separate the influence of population effects and individual cellular characteristics in setting networks' phase resetting properties. Distributions of intrinsic properties among neurons coupled with mutual excitation may result in entities that have less erratic phase responses than the single neuron oscillators in our networks. Computational models of the lamprey swimming CPG and the pre-Bötzinger complex have found that populations with distributions of intrinsic properties have more robust firing properties than single neuron models (Hellgren et al. 1992; Butera et al. 1999b), but we are unaware of any study explicitly testing the phase resetting properties of biophysically realistic models of single neurons and populations. Assuming that individual cells in the spinal CPG could be identified experimentally, measurements of many cells' intrinsic properties would allow the distribution of parameter values to be estimated. The response of the network to stimulation of identified (classes of) neurons at various phases of the locomotor rhythm could also be measured, giving a sense of the CPG network's sensitivity to the activity of single (classes of) cells (Zelenin et al. 2001). One means of achieving this might be to use transgenic mouse lines in conjunction with technologies for optical control of neuronal excitability (channelrodopsin-2, photoswitchable activity label, etc.) to selectively activate or suppress populations of identified neurons at specific phases of the rhythm (Zhang et al. 2006; Szobota et al. 2007; Han and Boyden 2007; Fortin et al. 2008). The combined results of these experiments could aid in assessing the role of population effects on the phase resetting properties of the network.

Appendix: CPG model equations

Membrane voltage for model RGN cells is determined by spiking Na$^+$ and K$^+$ currents, a persistent sodium current, and a leak current:

$$\dot{V} = -(I_{\text{Na}} + I_{\text{K}} + I_{\text{NaP}} + I_{\text{L}} - I_{\text{app}})/C \qquad (4)$$

while the equation governing MN and CIN cell membrane voltage omits the persistent sodium current:

$$\dot{V} = -(I_{\text{Na}} + I_{\text{K}} + I_{\text{L}} - I_{\text{app}})/C \qquad (5)$$

Membrane currents have the forms

$$I_{Na} = g_{Na}m_\infty^3(V)(1-n)(V-V_{Na}) \tag{6}$$

$$I_K = g_K n^4(V-V_K) \tag{7}$$

$$I_{NaP} = g_{NaP}m_{NaP_\infty}(V)h(V-V_{Na}) \tag{8}$$

$$I_L = g_L(V-V_L) \tag{9}$$

and dynamic activation variables are governed by equations of the form

$$\dot{y} = (y_\infty(V)-y)/\tau_y(V) \tag{10}$$

for $y \in \{h, n\}$.

Membrane voltage-dependent steady state equations for the (in)activation of the various currents have the form

$$x_\infty(V) = (1+\exp((V-\theta_x)/k_x))^{-1} \tag{11}$$

and the equations for voltage-dependent time constants have the form

$$\tau_y(V) = \overline{\tau}_y/\cosh[(V-\theta_y)/(2k_y)] \tag{12}$$

where $x \in \{m, m_{NaP}, h, n\}$ and $y \in \{h, n\}$.

References

Acker, C. D., Kopell, N., & White, J. A. (2003). Synchronization of strongly coupled excitatory neurons: Relating network behavior to biophysics. *Journal of Computational Neuroscience, 15*, 71–90.

Beato, M., & Nistri, A. (1999). Interaction between dishinhibited bursting and fictive locomotor patterns in the rat isolated spinal cord. *Journal of Neurophysiology, 82*(5), 2029–2038.

Beierholm, U., Nielsen, C. D., Ryge, J., Alstrøm, P., & Kiehn, O. (2001). Characterization of reliability of spike timing in spinal interneurons during oscillating inputs. *Journal of Neurophysiology, 86*(4), 1858–1868.

Best, J., Borisyuk, A., Rubin, J., Terman, D., & Wechselberger, M. (2005). The dynamic range of bursting in a model respiratory pacemaker network. *SIAM Journal of Applied Dynamical Systems, 4*(4), 1107–1139.

Birinyi, A., Viszokay, K., Wéber, I., Kiehn, O., & Antal, M. (2003). Synaptic targets of commissural interneurons in the lumbar spinal cord of neonatal rats. *Journal of Comparative Neurology, 461*, 429–440.

Bracci, E., Beato, M., & Nistri, A. (1997). Afferent inputs modulate the activity of a rhythmic burst generator in the rat disinhibited spinal cord *in vitro*. *Journal of Neurophysiology, 77*(6), 3157–3167.

Bracci, E., Beato, M., & Nistri, A. (1998). Extracellular K$^+$ induces locomotor-like patterns in the rat spinal cord *in vitro*: Comparison with NMDA or 5-HT induced activity. *Journal of Physiology, 79*(5), 2643–2652.

Brownstone, R. M., & Wilson, J. M. (2008). Strategies for delineating spinal locomotor rhythm-generating networks and the possible role of Hb9 interneurones in rhythmogenesis. *Brain Research Reviews, 57*(1), 64–76.

Buono, P. L. (2001). Models of central pattern generators for quadruped locomotion II. Secondary gaits. *Journal of Mathematical Biology, 42*, 327–346.

Buono, P. L., & Golubitsky, M. (2001). Models of central pattern generators for quadruped locomotion I. Primary gaits. *Journal of Mathematical Biology, 42*, 291–326.

Butera, R. J., Rinzel, J., & Smith, J. C. (1999a). Models of respiratory rhythm generation in the pre-Bötzinger complex. I. Bursting pacemaker neurons. *Journal of Neurophysiology, 81*, 382–397.

Butera, R. J., Rinzel, J., & Smith, J. C. (1999b). Models of respiratory rhythm generation in the pre-Bötzinger complex. II. Populations of coupled pacemaker neurons. *Journal of Neurophysiology, 81*, 398–415.

Butt, S. J. B., & Kiehn, O. (2003). Functional identification of interneurons responsible for left-right coordination of hindlimbs in mammals. *Neuron, 38*, 953–963.

Butt, S. J. B., Lebret, J. M., & Kiehn, O. (2002). Organization of left-right coordination in the mammalian locomotor network. *Brain Research Reviews, 40*, 107–117.

Butt, S. J. B., Lundfald, L., & Kiehn, O. (2005). EphA4 defines a class of excitatory locomotor-related interneurons. *Proceedings of the National Academy of Sciences, 102*(39), 14098–14103.

Cazalets, J. R., & Bertrand, S. (2000). Ubiquity of motor networks in the spinal cord of vertebrates. *Brain Research Bulletin, 53*(5), 627–634.

Cazalets, J. R., Borde, M., & Clarac, F. (1995). Localization and organization of the central pattern generator for hindlimb locomotion in the newborn rat. *Journal of Neuroscience, 15*(7), 4943–4951.

Cazalets, J. R., Borde, M., & Clarac, F. (1996). The synaptic drive from the spinal locomotor network to motoneurons in the newborn rat. *Journal of Neuroscience, 16*(1), 298–306.

Christie, K. J., & Whelan, P. J. (2005). Monoaminergic establishment of rostrocaudal gradients of rhythmicity in the neonatal mouse spinal cord. *Journal of Neurophysiology, 94*, 1554–1564.

Clewley, R., Sherwood, W. E., Lamar, M. D., & Guckenheimer, J. (2007). PyDSTool: an integrated simulation, modeling, and analysis package for dynamical systems. http://sourceforge.net/projects/pydstool/.

Cowley, K. C., & Schmidt, B. J. (1997). Regional distribution of the locomotor pattern-generating network in the neonatal rat spinal cord. *Journal of Neurophysiology, 77*(1), 247–259.

Crone, S. A., Quinlan, K. A., Zagoraiou, L., Droho, S., Restrepo, C. E., Lundfald, L., et al. (2008). Genetic ablation of V2a ipsilateral interneurons disrupts left-right locomotor coordination in mammalian spinal cord. *Neuron, 60*, 70–83.

Crone, S. A., Zhong, G., Harris-Warrick, R., & Sharma, K. (2009). In mice lacking V2a interneurons, gait depends on speed of locomotion. *Journal of Neuroscience, 29*(21), 7098–7109.

Daun, S., Rubin, J. E., & Rybak, I. A. (2009). Control of oscillation periods and phase durations in half-center central pattern generators: A comparative mechanistic analysis. *Journal of Computational Neuroscience, 27*(1), 3–36.

De Vries, G., & Sherman, A. (2005). Beyond synchronization: Modulatory and emergent effects of coupling in square-wave bursting. In S. Coombes & P. C. Bressloff (Eds.), *Bursting: The genesis of rhythm in the nervous system* (Chap. 4, pp. 243–272). World Scientific.

Destexhe, A., Mainen, Z. F., & Sejnowski, T. J. (1994). Synthesis of models for excitable membranes, synaptic transmission and neuromodulation using a common kinetic formalism. *Journal of Computational Neuroscience, 1*, 195–230.

Destexhe, A., Mainen, Z. F., & Sejnowski, T. J. (1998). Kinetic models of synaptic transmission. In C. Koch & I. Segev (Eds.), *Methods in neuronal modeling: From ions to networks* (2nd ed., Chap. 1, pp. 1–26). The MIT Press.

Dottori, M., Hartley, L., Galea, M., Paxinos, G., Polizzotto, M., Kilpatrick, T., et al. (1998). EphA4 (Sek1) receptor tyrosine kinase is required for the development of the corticospinal tract. *Proceedings of the National Academy of Sciences, 95*, 13248–13253.

Eide, A. L., Glover, J., Kjaerulff, O., & Kiehn, O. (1999). Characterization of commissural interneurons in the lumbar region of the neonatal rat spinal cord. *Journal of Comparative Neurology, 403*, 332–345.

Endo, T., & Kiehn, O. (2008). Asymmetric operation of the locomotor central pattern generator in the neonatal mouse spinal cord. *Journal of Neurophysiology, 100*, 3043–3054.

Fortin, D. L., Banghart, M. R., Dunn, T. W., Borges, K., Wagenaar, D. A., Gaudry, Q., et al. (2008). Photochemical control of endogenous ion channels and cellular excitability. *Nature Methods, 5*(4), 331–338.

Golubitsky, M., Josic, K., & Shea-Brown, E. (2006). Winding numbers and average frequencies in phase oscillator networks. *Journal of Nonlinear Science, 16*, 201–231.

Golubitsky, M., & Stewart, I. (2006). Nonlinear dynamics of networks: The groupoid formalism. *Bulletin of the American Mathematical Society, 43*(3), 305–364.

Golubitsky, M., Stewart, I., Buono, P. L., & Collins, J. J. (1998). A modular network for legged locomotion. *Physica D, 115*, 56–72.

Golubitsky, M., Stewart, I., Buono, P. L., & Collins, J. J. (1999). Symmetry in locomotor central pattern generators and animal gaits. *Nature, 401*, 693–695.

Goulding, M., & Pfaff, S. L. (2005). Development of circuits that generate simple rhythmic behaviors in vertebrates. *Current Opinion in Neurobiology, 15*, 14–20.

Grillner, S. (1981). Control of locomotion in bipeds, tetrapods, and fish. In *Handbook of physiology. The nervous system. Motor control* (Vol. II, Chap. 26, pp. 1179–1236). Bethesda, MD: American Physiological Society.

Grillner, S. (2003). The motor infrastructure: From ion channels to neuronal networks. *Nature Reviews Neuroscience, 4*, 573–586.

Guckenheimer, J., & Meloon, B. (2000). Computing periodic orbits and their bifurcations with automatic differentiation. *SIAM Journal of Scientific Computing, 22*(3), 951–985.

Hairer, E., & Wanner, G. (1991). Solving ordinary differential equations II: Stiff and differential-algebraic problems. In *Springer series in computational mathematics*. Berlin: Springer.

Han, X., & Boyden, E. S. (2007). Multiple-color optical activation, silencing, and desynchronization of neural activity, with single-spike temporal resolution. *PLoS ONE, 3*(e299), 1–12.

Hellgren, J., Grillner, S., & Lansner, A. (1992). Computer simulation of the segmental neural network generating locomotion in lamprey by using populations of network interneurons. *Biological Cybernetics, 68*(1), 1–13.

Hinckley, C. A., Hartley, R., Wu, L., Todd, A., & Ziskand-Conhaim, L. (2005). Locomotor-like rhythms in a genetically distinct cluster of interneurons in the mammalian spinal cord. *Journal of Neurophysiology, 93*, 1439–1449.

Hochman, S., Jordan, L. M., & MacDonald, J. F. (1994). N-methy-D-aspartate receptor-mediated voltage oscillations in neurons surrounding the central canal in slices of rat spinal cord. *Journal of Neurophysiology, 72*(2), 565–577.

Hultborn, H., Conway, B. A., Gossard, J. P., Brownstone, R., Fedirchuk, B., Schomburg, E. D., et al. (1998). How do we approach the locomotor network in the mammalian spinal cord? *Annals of the New York Academy of Sciences, 860*, 70–82.

Izhikevich, E. M. (2000). Neural excitability, spiking and bursting. *International Journal of Bifurcation and Chaos, 10*(6), 1171–1266.

Kiehn, O. (2006). Locomotor circuits in the mammalian spinal cord. *Annual Review of Neuroscience, 29*, 279–306.

Kiehn, O., & Butt, S. J. B. (2003). Physiological, anatomical and genetic identification of CPG neurons in the developing mammalian spinal cord. *Progress in Neurobiology, 70*, 347–361.

Kiehn, O., & Kjaerulff, O. (1996). Spatiotemporal characteristics of 5-HT and dopamine-induced rhythmic hindlimb activity in the *in vitro* neonatal rat. *Journal of Neurophysiology, 75*(4), 1472–1482.

Kiehn, O., & Kjaerulff, O. (1998). Distribution of central pattern generators for rhythmic motor outputs in the spinal cord of limbed vertebrates. *Annals of the New York Academy of Sciences, 860*, 110–129.

Kiehn, O., Kjaerulff, O., Tresch, M. C., & Harris-Warrick, R. M. (2000). Contributions of intrinsic motor neuron properties to the production of rhythmic motor output in the mammalian spinal cord. *Brain Research Bulletin, 53*(5), 649–659.

Kiehn, O., & Kullander, K. (2004). Central pattern generators deciphered by molecular genetics. *Neuron, 41*, 317–321.

Kiehn, O., Quinlan, K. A., Restrepo, C. E., Lundfald, L., Borgius, L., Talpalar, A. E., et al. (2008). Excitatory components of the mammalian locomotor CPG. *Brain Research Reviews, 57*, 56–63.

Kiehn, O., Sillar, K. T., Kjaerulff, O., & McDearmid, J. R. (1999). Effects of noradrenaline on locomotor rhythm-generating networks in the isolated neonatal rat spinal cord. *Journal of Neurophysiology, 82*, 741–746.

Kjaerulff, O., & Kiehn, O. (1993). Distribution of networks generating and coordinating locomotor activity in the neonatal rat spinal cord *in vitro*: A lesion study. *Journal of Neuroscience, 16*(18), 5777–5794.

Kjaerulff, O., & Kiehn, O. (1997). Crossed rhythmic synaptic input to motoneurons during selective activation of the contralateral spinal locomotor network. *Journal of Neuroscience, 17*(24), 9433–9447.

Kjaerulff, O., & Kiehn, O. (2001). 5-HT modulation of multiple inward rectifiers in motoneurons in intact preparations of the neonatal rat spinal cord. *Journal of Neurophysiology, 85*, 850–593.

Kremer, E., & Lev-Tov, A. (1997). Localization of the spinal network associated with generation of hindlimb locomotion in the neonatal rat and organization of its transverse coupling system. *Journal of Neurophysiology, 77*, 1155–1170.

Kullander, K. (2005). Genetics moving to neuronal networks. *TRENDS in Neurosciences, 28*(5), 239–247.

Kullander, K., Butt, S. J. B., Lebret, J. M., Lundfald, L., Restrepo, C., Rydström, A., et al. (2003). Role of EphA4 and EphrinB3 in local neuronal circuits that control walking. *Science, 299*(5614), 1889–1892.

Kuo, J. J., Lee, R. H., Zhang, L., & Heckman, C. J. (2006). Essential role of the persistent sodium current in spike initiation during slowly rising inputs in mouse spinal neurones. *Journal of Physiology, 574*(3), 819–834.

Lafreniere-Roula, M., & McCrea, D. A. (2005). Deletions of rhythmic motoneuron activity during fictive locomotion and scratch provide clues to the organization of the mammalian central pattern generator. *Journal of Neurophysiology, 94*, 1120–1132.

Lansner, A., Kotaleski, J. H., & Grillner, S. (1998). Modeling of the spinal neuronal circuitry underlying locomotion in a lower vertebrate. *Annals of the New York Academy of Sciences, 860*, 239–249.

Lanuza, G. M., Gosgnach, S., Pierani, A., Jessell, T. M., & Goulding, M. (2004). Genetic identification of spinal interneurons that coordinate left-right locomotor activity necessary for walking movements. *Neuron, 42*, 375–386.

Lee, R. H., & Heckman, C. J. (2000). Adjustable amplification of synaptic input in the dendrites of spinal motoneurons *in vivo*. *Journal of Neuroscience, 20*(17), 6734–6740.

McCrea, D. A., & Rybak, I. A. (2007). Modeling the mammalian locomotor CPG: Insights from mistakes and perturbations. *Progress in Brain Research, 165*, 235–253.

Nadim, F., Olsen, Ø. H., De Schutter, E., & Calabrese, R. L. (1995). Modeling the leech heartbeat elemental oscillator. I. Interactions of intrinsic and synaptic currents. *Journal of Computational Neuroscience, 2*, 215–235.

Nishimaru, H., & Kudo, N. (2000). Formation of the central pattern generator for locomotion in the rat and mouse. *Brain Research Bulletin, 53*(5), 661–669.

Nishimaru, H., Restrepo, C. E., & Kiehn, O. (2006). Activity of renshaw cells during locomotor-like rhythmic activity in the isolated spinal cord of neonatal mice. *Journal of Neuroscience, 26*(20), 5320–5328.

Pearson, K. G., & Rossignol, S. (1991). Fictive motor patterns in chronic spinal cats. *Journal of Neurophysiology, 66*(6), 1874–1887.

Phipps, E. T. (2003). *Taylor series integration of differential algebraic equations: automatic differentiation as a tool for simulating rigid body mechanical systems*. Ph.D. thesis, Cornell University.

Pinto, C. M. A., & Golubitsky, M. (2006). Central pattern generators for bipedal locomotion. *Journal of Mathematical Biology, 53*, 474–489.

Prinz, A. A., Thirumalai, V., & Marder, E. (2003). The functional consequences of changes in the strength and duration of synaptic inputs to oscillatory neurons. *Journal of Neuroscience, 23*(3), 943–954.

Puskár, Z., & Antal, M. (1997). Localization of last-order premotor interneurons in the lumbar spinal cord of rats. *Journal of Comparative Neurology, 389*, 377–389.

Quinlan, K. A., & Kiehn, O. (2007). Segmental, synaptic actions of commissural interneurons in the mouse spinal cord. *Journal of Neuroscience, 27*(24), 6521–6530.

Raastad, M., Enríquez-Denton, M., & Kiehn, O. (1998). Synaptic signaling in an active central network only moderately changes passive membrane properties. *Proceedings of the National Academy of Sciences, 95*(17), 10251–10256.

Raastad, M., Johnson, B. R., & Kiehn, O. (1997). Analysis of EPSCs and IPSCs carrying rhythmic, locomotor-related information in the isolated spinal cord of the neonatal rat. *Journal of Neurophysiology, 78*, 1851–1859.

Raastad, M., & Kiehn, O. (2000). Spike coding during locomotor network activity in ventrally located neurons in the isolated spinal cord from neonatal rat. *Journal of Neurophysiology, 83*, 2825–2834.

Rinzel, J. (1987). A formal classification of bursting mechanisms in excitable systems. In E. Teramoto & M. Yamaguti (Eds.), *Mathematical topics in population biology, morphogenesis and neurosciences. Lecture notes in biomathematics* (Vol. 71, pp. 267–281). Berlin: Springer.

Rinzel, J., & Lee, Y. S. (1987). Dissection of a model for neuronal parabolic bursting. *Journal of Mathematical Biology, 25*, 653–675.

Rowat, P. F., & Selverston, A. I. (1997). Oscillatory mechanisms in pairs of neurons connected with fast inhibitory synapses. *Journal of Computational Neuroscience, 4*, 103–127.

Rybak, I. A., Shevtsova, N. A., Lafreniere-Roula, M., & McCrea, D. A. (2006a). Modelling spinal circuitry involved in locomotor pattern generation: Insights from the effects of afferent stimulation. *Journal of Physiology, 577*(2), 641–658.

Rybak, I. A., Stecina, K., Shevtsova, N. A., & McCrea, D. A. (2006b). Modelling spinal circuitry involved in locomotor pattern generation: Insights from deletions during fictive locomotion. *Journal of Physiology, 577*(2), 617–639.

Sherman, A. (1994). Anti-phase, asymmetric and aperiodic oscillations in excitable cells—I. Coupled bursters. *Bulletin of Mathematical Biology, 56*(5), 811–835.

Sherwood, W. E. (2008). *Phase response in networks of bursting neurons: Modeling central pattern generators*. Ph.D. thesis, Cornell University.

Sherwood, W. E., & Guckenheimer, J. (2010). Dissecting the phase response of a model bursting neuron. *SIAM Journal of Applied Dynamical Systems, 9*(3), 659–768.

Skinner, F. K., Kopell, N., & Marder, E. (1994). Mechanisms for oscillation and frequency control in reciprocally inhibitory model neural networks. *Journal of Computational Neuroscience, 1*, 69–87.

Sqalli-Houssaini, Y., Cazalets, J. R., & Clarac, F. (1993). Oscillatory properties of the central pattern generator for locomotion in neonatal rats. *Journal of Neurophysiology, 70*(2), 803–813.

Stewart, I., Golubitsky, M., & Pivato, M. (2003). Symmetry groupoids and patterns of synchrony in coupled cell networks. *SIAM Journal of Applied Dynamical Systems, 2*(4), 609–646.

Stokke, M. F., Nissen, U. V., Glover, J. C., & Kiehn, O. (2002). Projection patterns of commissural interneurons in the lumbar spinal cord of the neonatal rat. *Journal of Comparative Neurology, 447*, 349–359.

Swift, J. W. (1988). Hopf bifurcation with the symmetry of the square. *Nonlinearity, 1*, 333–377.

Szobota, S., Gorostiza, P., Del Bene, F., Wyart, C., Fortin, D. L., Kolstad, K. D., et al. (2007). Remote control of neuronal activity with a light-gated glutamate receptor. *Neuron, 54*, 535–545.

Tazerart, S., Viemari, J. C., Darbon, P., Vinay, L., & Brocard, F. (2007). Contribution of persistent sodium current to locomotor pattern generation in neonatal rats. *Journal of Neurophysiology, 98*, 613–627. doi:10.1152/jn.00316.2007.

Tazerart, S., Vinay, L., & Brocard, F. (2008). The persistent sodium current generates pacemaker activities in the central pattern generator for locomotion and regulates the locomotor rhythm. *Journal of Neuroscience, 28*(34), 8577–8589.

Tien, J. H. (2007). *Optimization for bursting neural models*. Ph.D. thesis, Cornell University.

Tresch, M. C., & Kiehn, O. (1999). Coding of locomotor phase in populations of neurons in rostral and caudal segments of the neonatal rat lumbar spinal cord. *Journal of Neurophysiology, 82*(6), 3563–3574.

Tresch, M. C., & Kiehn, O. (2000). Population reconstruction of the locomotor cycle from interneuron activity in the mammalian spinal cord. *Journal of Neurophysiology, 83*, 1972–1978.

Tresch, M. C., & Kiehn, O. (2002). Synchronization of motor neurons during locomotion in the neonatal rat: Predictors and mechanisms. *Journal of Neuroscience, 22*(22), 9997–10008.

Wilson, J. M., Dombeck, D. A., Díaz-Ríos, M., Harris-Warrick, R. M., & Brownstone, R. M. (2007). Two-photon

calcium imaging of network activity in xfp-expressing neurons in the mouse. *Journal of Neurophysiology, 97*, 3118–3125.

Wilson, J. M., Hartley, R., Maxwell, D. J., Todd, A. J., Lieberam, I., Kaltschmidt, J. A., et al. (2005). Conditional rhythmicity of ventral spinal interneurons defined by expression of the Hb9 homeodomain protein. *Journal of Neuroscience, 25*(24), 5710–5719.

Yakovenko, S., McCrea, D. A., Stechina, K., & Prochazka, A. (2005). Control of locomotor cycle durations. *Journal of Neurophysiology, 94*, 1057–1065.

Yokoyama, N., Romero, M. I., Cowan, C. A., Galvan, P., Helmbacher, F., Charnay, P., et al. (2001). Forward signaling mediated by ephrin-B3 prevents contralateral corticospinal axons from recrossing the spinal cord midline. *Neuron, 29*(1), 85–97.

Zelenin, P. V., Grillner, S., Orlovsky, G. N., & Deliagina, T. G. (2001). Heterogeneity of the population of command neurons in the lamprey. *Journal of Neuroscience, 21*(19), 7793–7803.

Zhang, F., Wang, L. P., Boyden, E. S., & Deisseroth, K. (2006). Channelrhodopsin-2 and optical control of excitable cells. *Nature Methods, 3*(10), 785–792.

Zhong, G., Díaz-Ríos, M., & Harris-Warrick, R. M. (2006a). Intrinsic and functional differences among commissural interneurons during fictive locomotion and serotonergic modulation in the neonatal mouse. *Journal of Neuroscience, 26*(24), 6509–6517.

Zhong, G., Díaz-Ríos, M., & Harris-Warrick, R. M. (2006b). Serotonin modulates the properties of ascending commissural interneurons in the neonatal mouse spinal cord. *Journal of Neurophysiology, 95*, 1545–1555.

Zhong, G., Masino, M. A., & Harris-Warrick, R. M. (2007). Persistent sodium currents participate in fictive locomotion generation in neonatal mouse spinal cord. *Journal of Neuroscience, 27*(17), 4507–4518.

Ziskand-Conhaim, L., Wu, L., & Wiesner, E. P. (2008). Persistent sodium current contributes to induced voltage oscillations in locomotor-related Hb9 interneurons in the mouse spinal cord. *Journal of Neurophysiology, 100*, 2254–2264.